Highlights

- A fully coupled model was proposed for the migration of VOCs in unsaturated landfill liners.
- Finite deformation of soil was considered in the new model.
- The transport of gas phase VOCs was found to dominate the migration progress.
- The temperature gradient can accelerate the breakthrough of VOCs in an unsaturated liner.
- The mechanical consolidation slowed down the motion of the VOCs.

Migration of volatile organic contaminations (VOCs) through a deforming clay liner

H. J. Zhang[1], D.-S. Jeng[2,#], D. A. Barry[3], B. R. Seymour[4] and L. Li[5]

[1] *Faculty of Civil Engineering and Mechanics, Jiangsu University, Zhenjiang, 212013, Jiangsu, China*
[2] *Griffith School of Engineering, Griffith University Gold Coast Campus, QLD 4222, Australia*
[3] *Laboratoire de technologie écologique, Faculté deL'environnement naturel, architectural et construit (ENAC), Station 2, Ecole polytechnique fédérale de lausanne (EPFL), 1015 Lausanne, Switzerland*
[4] *Department of Mathematics, University of British Columbia, Vancouver BC, V6T 1Z2, Canada*
[5] *National Centre for Groundwater Research and Training, School of Civil Engineering, The University of Queensland, St. Lucia, QLD 4072, Australia*
[#] *Corresponding author, email: jengd2@asme.org*

Abstract

A fully coupled thermal–hydraulic–mechanical–chemical (THMC) model was proposed to describe the migration of volatile organic contaminations (VOCs) in unsaturated landfill liners. The vertical soil stress, capillary pressure, air pressure, temperature increase, and solute concentration were selected as the primary variables. Finite deformations were described using Lagrangian coordinates. Non-isothermal moisture transport was found to be dependent on both the temperature gradient and the concentration of the VOCs. The VOCs were assumed to exist and be transported in three phases in the soil: solid, liquid, and gas. An illustrative example of an unsaturated landfill with a compacted clay liner was presented. For the case considered, the transport of gas phase VOCs was found to dominate the migration progress. Moreover, the temperature gradient can accelerate the breakthrough of VOCs in an unsaturated liner, while the mechanical consolidation slowed down the motion of the VOCs.

Keywords: Material coordinate, multi-phase, heat energy transfer, large deformation

1. Introduction

Solid waste landfills can pose major environmental threats to the quality of groundwater resources. Unlike inorganic compounds, VOCs can diffuse through the geomembrane, then breakthrough the underlying barrier and contaminate the surrounding groundwater. Understanding the progress and minimizing the migration of VOCs in landfill liners aids both barrier design and analysis of existing landfills.

Most research in the area has focused on the transport of the liquid phase. For example, Kim [1] modeled VOC solute transport through a leachate drainage layer overlying a geomembrane and the compacted soil layer underneath. The leaked leachate was approximated as uniform flow over the whole surface area of soil liner. The seepage velocity was evaluated by an equivalent hydraulic gradient, which depends on the height of the leachate level accumulated on the geomembrane. The medium was considered to be fully saturated with dissolved VOC due to aqueous phase advection and diffusion. Nguyen et al. [2] compared the performance of different composite liner systems based on the diffusion of VOCs in the liquid phase through a fully saturated liner. In reality, the basal soil liner is always unsaturated [3]. Fityus et al. [3] employed a steady-state unsaturated moisture distribution to model the mass transfer through a partially saturated soil liner incorporating only the liquid phase. However, VOCs can reside in the gas phase in addition to the solid and liquid phases [4]. Therefore, gas-phase motion in the pores of an unsaturated soil liner and its contribution to VOC migration should be investigated to ascertain its contribution to VOC transport in landfills.

Moisture transport in unsaturated soils is affected by temperature gradients, which, for example, can cause liquid-to-vapour phase changes and vice versa, as well as vapour phase transport. A series of laboratory experiments were carried out by Nassar et al. [5] to investigate heat, water, potassium chloride, and benzene transport in unsaturated soils under isothermal and non-isothermal conditions. They concluded that the effect of temperature and temperature gradients should be included to describe the movement of volatile chemicals in soils.

Although the temperature generated by the breakdown of solid waste in a landfill is not in general extremely high (between 30 °C and 60 °C [6]), the transport of volatile organics can be influenced by different factors:

(1) The temperature gradient can act as a driving force in moisture transport. Especially for unsaturated soil with a connected pore air phase, the moisture flow caused by water vapour density variations can play an important role [7]. In this case, multi-phase flow modelling is necessary.

(2) Further, a rising temperature influences the contaminant transport due to its effect on the gaseous mixture of water vapour, dry air and VOC gas. Therefore, generally speaking, non-isothermal multi-phase moisture flow should be included in modelling VOC transport within an unsaturated landfill clay liner with inter-connected pore air.

An analytical solution is available for volatile organic contamination (VOC) transport in a porous medium [8]. Not surprisingly, it includes several assumptions and does not account for transient fluid and gas velocities induced by consolidation and temperature gradients. For such phenomena, numerical models are

essential. Some progress has been made using numerical solutions to couple non-isothermal moisture flow with solute or toxic gas transport in unsaturated soils. For example, Nassar and Horton [9] included three fully-coupled partial differential equations connecting the heat, water, and solute transfer to describe their simultaneous transfer in a rigid unsaturated soil. Thomas and Ferguson [10] developed a fully coupled heat and mass transfer model describing the migration of liquid water, heat, air, and contaminant gas through an engineered clay liner, but without including deformations.

Small soil deformations were incorporated for non-isothermal moisture transport in an unsaturated landfill liner [11, 12]. However, small-deformation models could overestimate the transit time of contaminants across a landfill liner with increasing discrepancies for increasing compressibility of the liner [13]. Therefore, finite deformation formulations should generally be utilized to address the geometric non-linearity [14, 15].

In summary, existing models of the migration of VOCs in landfill soil liners have at least one of the following assumptions:

1. The soil liner is under an isothermal condition;
2. The soil liner is fully saturated;
3. VOC transport occurs only in the liquid phase although the soil liner is unsaturated;
4. The soil liner is rigid;
5. The soil liner deformation is determined by a small-strain model.

Meanwhile, there is increasingly more interest in VOC emissions through the landfill cover [16, 17, 18], because the landfill emissions are regulated based on

emissions of non-methane organic compounds rather than methane in some countries (for instance, in the US). Landfills generally have three types of covers: daily, intermediate, and final. Many daily covers are approximately 30cm thick exposed layers of clay soil over refuse. Therefore, there is a strong desire to model VOC through soils experiencing temperature gradients with variable water saturation.

To overcome these restrictions, the present study proposes a mathematical model for non-isothermal, multi-phase moisture and VOC transport (in solid, liquid and gas phases) for unsaturated soil, incorporating finite deformations. The model is benchmarked against an example of isothermal moisture transport in a soil column and an analytical solution describing multi-phase VOC transport in unsaturated soil. Then, the breakthrough of the VOCs in an unsaturated CCL (Compacted Clay Liner) is examined. The influences of various factors such as mechanical consolidation, the temperature gradient, the soil velocity, finite deformations, mechanical dispersion, and the water vapour diffusivity in the presence of VOC vapour are investigated. The contribution of dispersion (diffusion and mechanical dispersion) in the gas phase is also examined.

2. Model Formulation

The main processes considered are mechanical consolidation, and moisture, VOC and heat transport. Correspondingly, the model consists of an equilibrium of forces for the solid phase, mass balances for moisture, gas and VOC, and balance of energy. The primary variables selected are the capillary pressure, p_c, pore air pressure, p_a, increase of absolute temperature, T, and the liquid VOC mass concentration, c_l. In deriving the basic equations, the following assumptions are made:

1. The pore fluid flow in both the liquid and gas phases are driven by pressure, viscous and gravity forces. Knudsen diffusion, which may become pronounced when the gas molecules collide primarily with the pore walls rather than with other molecules [19], is not accounted for in this work, because the gas permeability coefficient of CCL considered is 10^{-12} m^2 and thus much greater than the threshold value of 10^{-14} m^2[20]. Also, data associated with the Knudsen diffusion coefficient and its variation with water content and temperature are not available for CCL experiments.
2. Diffusion and convection drive the movement of the water vapour. To model the multicomponent gas mixtures, the dusty gas model including the Knudsen diffusion is frequently used [19]. An alternative approach [9], which is used in this paper, can be used when Knudsen diffusion can be neglected. Nassar and Horton's (1997) approach accounts for partial pressure gradients and binary gas-phase diffusion, which are important factors for multicomponents gas.
3. Heat flow occurs by conduction and convection and boiling, freezing, and thawing are not considered [9]. The approximation of local thermal equilibrium is used which means all phases within a representative element volume (REV) of soil have the same temperature. This assumption is acceptable as the energy exchange between the phases is significantly faster than the energy transport within a phase. This is valid for small grain sizes and their linked large specific soil surface area between the phases [21].
4. The soil liner is intact, namely there is no presence of inorganic pollutant or the associated chemical reactions with soil liner. Sorption is assumed not to change the soil porosity.

2.1. Coordinate systems

A Lagrangian coordinate system (z, t) is used with $\xi(z,t)$ as the particle displacement and $\xi(z,0) = z$. The relation between the Lagrangian and Eulerian (ξ, t) coordinate systems then implies that for any variable $F(z,t) = f(\xi(z,t),t)$:

$$\frac{\partial F}{\partial z} = \frac{\partial f}{\partial \xi}\frac{\partial \xi}{\partial z}, \quad \frac{\partial F}{\partial t} = \frac{\partial f}{\partial \xi}\frac{\partial \xi}{\partial t} + \frac{\partial f}{\partial t} = \frac{\partial f}{\partial \xi}v_s + \frac{\partial f}{\partial t}, \tag{1}$$

where $v_s = \partial\xi/\partial t$ is the solid velocity.

Since the same amount of solid remains in each soil representative elementary volume (REV), the continuity equation for the solid phase takes the form:

$$\rho_s(z,0)(1-n_0)\Delta z = \rho_s(1-n)\Delta\xi, \tag{2}$$

where ρ_s is the soil grain density, $n = e/(1+e)$ is the current porosity, and $n_0 = n(z,0)$ is the initial porosity. The Jacobian, M, for the coordinate transformation is:

$$M = \frac{\partial \xi}{\partial z} = \frac{1-n_0}{1-n} = \frac{1+e}{1+e_0}, \tag{3}$$

where e_0 is the initial void ratio.

2.2. Force equilibrium

The lateral soil pressure, σ_l is related to the vertical pressure, σ_v by the earth pressure coefficient at rest, K_0 [22, 23, 24]:

$$\sigma_l + p_a = K_0(\sigma_v + p_a). \tag{4}$$

Hence, the net mean stress is:

$$\sigma^* = \frac{\sigma_v + 2\sigma_l}{3} + p_a = \frac{1 + 2K_0}{3}\sigma_v + p_a. \quad (5)$$

Here, the tension stresses are taken as positive and p_a is the pore air gauge pressure.

For the compaction-induced soil lateral pressure, the value of K_0 increases rapidly with the degree of saturation around the optimum water content, and may exceed 0.9 when the water content is above the optimum [24]. In engineering practice, the landfill clay liner is required to be compacted with the water content usually above the optimum [25]. Therefore, K_0 is taken as 0.9 in this study.

The force equilibrium of the soil is described in terms of vertical soil stress σ_v by:

$$\frac{\partial \sigma_v}{\partial z} - b\frac{\partial \xi}{\partial z} = 0, \quad (6)$$

where b denotes the body force:

$$b = \{[\theta\rho_l + (1-n)\rho_s] - [\theta_0\rho_l + (1-n_0)\rho_s]\}\, g_i. \quad (7)$$

Here, θ and θ_0 represent the current and initial water volume fractions, respectively, ρ_l denotes the density of liquid water, g_i is the gravitational vector taken with positive being upwards (and equals the acceleration due to gravity g, when the vertical coordinate, z, is opposite the direction of gravity; otherwise, $g_i = -g$). The masses of dry air and water vapour are negligibly small and are ignored.

2.3. Moisture and heat energy transfer in the spatial coordinate system (ξ, t)

2.3.1. Mass balance for water

The liquid water and water vapour flux in an unsaturated media can be written as:

$$q_l = \rho_l \theta v_{li} - \rho_l D_T \frac{\partial T}{\partial \xi}, \tag{8}$$

$$q_v = -D^* \frac{\partial \rho_v}{\partial \xi} + \rho_v (n - \theta) v_{ai}. \tag{9}$$

The second term on the right-hand side (RHS) of (8) represents the water flux due to the thermal gradient, D_T is a phenomenological coefficient relating the water flux to the temperature gradient, T is the absolute temperature increase, and D^* describes the effective molecular diffusivity of the water vapour. According to Darcy's law, the intrinsic or linear average velocity of each individual liquid phase in soil is:

$$v_{li} = -\frac{k_l}{\theta} \frac{\partial}{\partial \xi} (p_c + p_a + \rho_l g_i \xi) + v_s, \tag{10}$$

$$v_{ai} = -\frac{k_a}{n - \theta} \frac{\partial p_a}{\partial \xi} + v_s, \tag{11}$$

where k_l and k_a are the mobility coefficients for the liquid pore water and continuous air phases, respectively, $k_l = K_l/(\rho_l g)$, in which K_l is the hydraulic conductivity of the soil medium and v_{li} and v_{ai} denote the intrinsic phase average velocity with respect to a fixed coordinate system [26] for liquid and vapour water, respectively. The gravitational contribution to v_{ai} is neglected because the density of air ρ_a is negligibly small [27].

The importance of the compressibility of pore water was demonstrated in the prediction of solute breakthrough curves from partially saturated landfill liners [28]. The solute was assumed to exist in the solid and liquid phases. For the multi-phase VOC transport model in this study, the density of both liquid and vapour water are taken as functions of temperature and capillary pressure:

$$\rho_l = \rho_{l0}\left[1 + \beta_l\left(p_c + p_a\right) - \alpha_l T\right], \tag{12}$$

where the initial density of liquid water is $\rho_{l0} = 998$ kg/m^3, the pore water compressibility coefficient $\beta_l = 3.3 \times 10^9$ Pa^{-1}, and $\alpha_l = 3.0 \times 10^{-4}$ K^{-1} [27],

$$\rho_v = \rho_0 h = \rho_0 \exp\left[\frac{p_c}{\rho_l R_v\left(T + T_0\right)}\right], \tag{13}$$

in which h is relative humidity and ρ_0 is the density of vapour at saturation given by [29]:

$$\rho_0 = \frac{1}{194.4}\exp\left[a_0 T' + b_0\left(T'\right)^2\right], \tag{14}$$

where $a_0 = 0.06374$, $b_0 = -0.1634 \times 10^{-3}$, $T' = T + T_0 - 273$, and T_0 is the initial temperature (K assumed).

In earlier non-isothermal moisture transport models [30, 29, 11, 27, 12], the solid velocity was not included in the expression for the water flux in deformable media. Here, the solid velocity is incorporated in both the mass and heat fluxes, and also in the liquid linear average velocity. When converted to the material coordinate system in the next section, all terms involving v_s are found to disappear and no extra complexity in the formulas is introduced.

The mass conservation equation for the moisture in a deformable unsaturated soil is:

$$\frac{\partial}{\partial t}\left[\rho_l\theta + \rho_v(n-\theta)\right] = -\frac{\partial}{\partial \xi}\left(q_l + q_v\right). \tag{15}$$

Zhou et al. [27] took D_T as 2.4×10^{-10} m^2/(s K) in their example of a non-isothermal unsaturated soil column, while other researchers have attributed the influence of the temperature on the liquid water flux to its effect on the capillary potential head, expressed as [9, 7]:

$$D_T = k_l \rho_l g \frac{\partial \Psi}{\partial T}. \tag{16}$$

The temperature-corrected potential head, assumed to be a function of the capillary potential head, Ψ, and the temperature, is given by [31]:

$$\Psi = \frac{p_c}{\rho_l g}\exp(-C_\psi T), \tag{17}$$

where C_ψ= -0.0068 K^{-1}is the temperature coefficient of water retention [32, 33].

Considering a gaseous mixture of dry air and water vapour, the effective molecular diffusivity of the water vapour, D^*, can be expressed as [7, 27]:

$$D^* = D_{atm} \nu_m \tau (n-\theta), \tag{18}$$

where τ is the dimensionless tortuosity factor to account for complexities in the pore geometry and the boundary conditions that influence the vapour transport at the microscopic scale. Its typical value is less than unity for intact soil, and it is temperature dependent [27]. The mass flow factor is defined as $\nu_m = p_a/(p_a - p_v)$. D_{atm} is the molecular diffusion coefficient of water vapour in air (m^2/s), and is expressed in terms of absolute temperature and air pressure (here, p_a is in units of Pa) [29]:

$$D_{atm} = 5.893 \times 10^{-6} \frac{(T + T_0)^{2.3}}{p_a}. \tag{19}$$

Alternatively, the diffusion flux of vapour, which is assumed to be driven by the vapour density gradient [11], can be described by an extended vapour velocity equation [34]:

$$D^* \frac{\partial \rho_v}{\partial \xi} = n D_{atm} \nu_m \left[\frac{\partial \rho_v}{\partial p_c} \frac{\partial p_c}{\partial \xi} + \frac{(\nabla T)_a}{\nabla T} \frac{\partial \rho_v}{\partial T} \frac{\partial T}{\partial \xi} \right], \tag{20}$$

where $(\nabla T)_a / \nabla T$ is the ratio of the microscopic to the macroscopic temperature gradient. It is introduced since the microscopic temperature gradients in the fluid-filled pores are much higher than the macroscopic gradients across the sample as a whole. Thomas and Ferguson [10] employed (20) to describe the water vapour diffusivity even in the presence of VOC gas.

When the concentration of the VOCs in the liquid phase increases to a critical level, its effect on Ψ cannot be neglected. It is considered via the surface tension model [35]:

$$\Psi = \Psi(T_r)(\gamma_m / \gamma_w), \tag{21}$$

where T_r is an arbitrary reference temperature, $\Psi(T_r)$ is the capillary pressure head at the reference temperature, γ_w is the surface tension of a free-water system at the reference temperature (J/m^2), and γ_m is the surface tension (J/m^2) at a VOC concentration of c_l. In view of (17), the capillary pressure head can be expressed as:

$$\Psi = \frac{p_c \gamma_m}{\rho_l g \gamma_w} \exp(-C_\psi T), \tag{22}$$

The effect of organic chemical concentrations on the surface tension, γ_m/γ_w, can be calculated for a nonionized organic solute by [36, 37]:

$$\frac{\gamma_m}{\gamma_w} = \left[\Gamma_w + \Gamma_0 \left(\gamma_0/\gamma_w\right)^{1/4}\right]^4, \tag{23}$$

where γ_0 is the surface tension of the VOCs (J/m^2), Γ_w and Γ_0 represent the superficial volume fraction of water and VOCs in the surface layer, for which data are rare in literature. Therefore, the effect of the VOCs on the surface tension of a mixed liquid is included by specifying a constant reduction factor for γ_m/γ_w. In contrast to inorganic species, organic compounds typically decrease the surface tension of water. The reduction factor falls within the range of 0.6 to 1 for organic concentrations lower than 10 mg/ml or less than 10^{-3} mol/ml [38, 39].

In the case of a gaseous mixture composed of water vapour, dry air, and VOC vapour, the water vapour diffusion may be influenced by the presence of the VOC vapour especially when its mole fraction is relatively large. It can be described by [36, 40]:

$$D^* = D_{wm} \left(n - \theta\right)^{5/3} \tag{24}$$

where the molecular diffusivity of water vapour in a gas mixture (m^2/s), D_{wm} is:

$$D_{wm} = \left(y_2'/D_{i-2} + y_3'/D_{i-3} + ... + y_n'/D_{i-n}\right)^{-1}, \tag{25}$$

in which D_{i-n} denotes the molecular diffusivity for the binary pair, i.e., water vapour diffusing through components n. y_n' is the mole fraction of component n in the gas mixture evaluated on a component-water-vapour-free basis, that is,

$$y_2' = \frac{y_2}{y_2 + y_3 + ... + y_n}. \tag{26}$$

For a gaseous mixture that obeys the ideal gas law, the mole fraction equals the ratio of the corresponding partial pressures [40].

2.3.2. Mass balance for dry air

Air flow occurs as a bulk flow and as a diffusive flow of dry air and the dissolved air within the pore water. Assuming that the diffusive flux of the dry air is very small relative to the bulk flow and can be ignored [11, 27], the mass balance for air in a deformable unsaturated soil can be written as:

$$\frac{\partial}{\partial t}\left\{\rho_{da}\left[n-(1-H)\,\theta\right]\right\}=-\frac{\partial q_{da}}{\partial \xi}, \tag{27}$$

where ρ_{da} is the density of dry air and H is the dimensionless coefficient of solubility defined by Henry's law [41]. The dry air flux, q_{da}, is described by:

$$q_{da}=H\rho_{da}\left(\theta v_{li}-D_T\frac{\partial T}{\partial \xi}\right)+\rho_{da}\,(n-\theta)\,v_{ai}. \tag{28}$$

Since the variation of the pore air pressure from the atmosphere pressure in this study is far less than 1 bar, except when the degree of saturation exceeds 0.985, and the temperature falls in the range of 283-333 K, the background condition is close to STP (standard temperature and pressure). It is then reasonable to assume that the gas mixture obeys the ideal gas law and Dalton's law [41, 11]. Therefore, we have:

$$\rho_{da}=\frac{p_{da}}{R_{da}\,(T+T_0)}, \tag{29}$$

$$p_v=\rho_v R_v\,(T+T_0)\,, \tag{30}$$

where $R_i(i=da,v)$ is the specific gas constant (the ideal gas constant divided by the molecular weight).

When the volume fraction of VOC in the gas phase is sufficiently small [42, 43, 44], it can be assumed that the presence of the VOCs does not significantly alter the density and pressure of the dry air and the water vapour. Applying Dalton's law to the pore air mixture, the pore air pressure p_a is the sum of the dry air pressure p_{da} and the vapour pressure p_v:

$$p_a = p_{da} + p_v. \tag{31}$$

Substituting (30) and (31) into (29) leads to:

$$\rho_{da} = \frac{p_a}{R_{da}\,(T + T_0)} - \frac{R_v}{R_{da}}\rho_v, \tag{32}$$

where the specific gas constant, $R_{da} = 287.1$ J/kg K, $R_v = 461.5$ J/kg K.

The above approach is applicable to the case with a relatively large VOC mole fraction in the gas mixture. Since the density of the VOC vapour (ρ_{VOC}) can be expressed in terms of the adsorption coefficient H and the liquid concentration of the VOCs, c_l, by $\rho_{VOC} = Hc_l$, this additional compound does not add an extra unknown. Using Dalton's law of partial pressure yields

$$p_{VOC} = \rho_{VOC} R_{VOC}\,(T + T_0)\,, \tag{33}$$

$$p_a = p_{da} + p_v + p_{VOC}, \tag{34}$$

and

$$\rho_{da} = \frac{p_a}{R_{da}\,(T + T_0)} - \frac{R_v}{R_{da}}\rho_v - -\frac{R_{VOC}}{R_{da}}\rho_{VOC}, \tag{35}$$

where R_{VOC} is the specific gas constant for the VOC.

2.3.3. Heat energy balance

For a unit volume of a deformable unsaturated medium, conservation of heat energy can be written as:

$$\frac{\partial \Phi}{\partial t} = -\frac{\partial q_T}{\partial \xi}, \tag{36}$$

where Φ and q_T are the heat capacity of the soil and the total heat flux per unit volume, respectively. Besides the heat content in an individual phase, considering the contributions of the latent heat of vapourization and exothermic process of wetting of the porous medium, Φ can be written as [27]:

$$\begin{aligned} \Phi = & \left[\rho_s(1-n)C_s + \rho_l\theta C_l + \rho_v\left(n-\theta\right)C_v + \rho_{da}\left(n-(1-H)\,\theta\right)C_{da}\right]T \\ & + L_0\rho_v\left(n-\theta\right) + \rho_l\theta W, \end{aligned} \tag{37}$$

where C_i $(i = s, l, v, da)$ is the specific heat capacity of each constituent in the soil, L_0 is the latent heat of vapourization, and W (J/kg) is the differential heat of wetting given by [31]:

$$W = \frac{H_w}{\rho_l \delta}\exp\left(-\frac{\theta}{\delta S'}\right), \tag{38}$$

in which $S' = 10^7$ m^{-1} is the specific surface of the material and the material constant values are H_w=1 J/m^2, $\delta = 10^{-9}$ m in accordance with [27].

Heat transfer mechanisms in our model include conduction, convection, the vapourization of heat, the gradient of the water potential, and the differential heat of the wetting flux. When expressing the gradient of the differential heat of wetting flux as the liquid water flux multiplied by the coefficient of the differential heat of wetting (W), q_T can be written as [45]:

$$q_T = -\lambda\frac{\partial T}{\partial \xi} + \left(\rho_s\left(1-n\right)v_s C_s + q_l C_l + q_v C_v + q_{da} C_{da}\right) T + q_l W + L_0 q_v - D_c^* \frac{\partial}{\partial \xi}\left(p_c + p_a + \rho_l g \xi_i\right), \tag{39}$$

where $\lambda = (1 - S_l)\lambda_{dry} + S_l\lambda_{sat}$ is the thermal conductivity (where the degree of saturation $S_l = \theta/n$, $\lambda_{dry} = 0.5$ J/(s m K), and $\lambda_{sat} = 2$ J/(s m K) [27]). $D_c^* = (T + T_0)D_T$ relates the water potential gradient to the heat flux [46, 47]. For the case where there is a relatively large VOC concentration in all three phases, the heat transfer parameters employed should be measured specifically to incorporate the effect of the VOCs.

2.3.4. Organic solute transfer

VOCs may reside in the soil in a liquid, gaseous, or a solid phase [4], and their transport can be due to diffusion and advection in both the liquid and vapour phases. Ignoring the degradation of the VOCs in the soil, their mass conservation is expressed as:

$$\frac{\partial c_{mt}}{\partial t} = -\frac{\partial q_{ct}}{\partial \xi}, \tag{40}$$

where c_{mt} denotes the mass of the contaminants per unit volume of the soil matrix, and q_{ct} represents the total VOC flux. In accordance with [36], we have:

$$c_{mt} = (1-n)\rho_s S + \theta c_l + (n-\theta)c_g, \tag{41}$$

where S is the adsorbed concentration (mass per mass soil) and can be divided into two parts [48], which is that sorbed from the water phase and from the air phase. Local chemical equilibrium is assumed between each phase, i.e., the concentration

of the VOCs in one phase can be evaluated from that in another phase. Assuming a linear partitioning coefficient between the soil phases i and j, H_{ij} [36, 5], we have

$$\begin{aligned} S &= H_{sl}c_l + H_{sg}c_g, \\ c_g &= H_{gl}c_l \end{aligned} \tag{42}$$

where c_i $(i = l, g)$ denotes the mass of the VOCs per unit volume of the liquid and gas phases, respectively. They are related by $H_{ij}(i, j = s, l, g)$, the linear partitioning coefficients between the individual soil phases. Nassar et al. [5] found that the liquid–solid partitioning coefficient, $H_{sl} = 0.343 \times 10^{-3}\text{m}^3/\text{kg}$ (which depends on the water mass content, kg water per kg soil), and the dimensionless Henry's constant, $H_{gl} = 0.2$ (which depends on the temperature and the relative humidity). The sorption of VOC from the vapour phase onto soil minerals, namely, H_{sg}, is strongly dependent upon the pore water content, the soil type, and the chemical properties of the sorbing VOC [5, 49]. It can be around 1,000 times the H_{sl} for dry soil [50]. H_{gl} for benzene is taken as 0.191 [51]. The partitioning coefficients are assumed to be functions of σ^*, p_c, p_a, and T for the sake of generality in the derivation of the related equations and coefficients. The linear sorption relationship employed here is valid because the concentrations of the VOCs in a landfill liner are normally very low [52, 48].

For the VOC transport mechanism, advection is caused by moisture transport (liquid and vapour) and by the solid grain motion for the deformable porous medium considered, while dispersion is caused by mechanical dispersion and molecular diffusion:

$$q_{ct} = -\theta D_{lc}\frac{\partial c_l}{\partial \xi} - (n-\theta)D_{gc}\frac{\partial c_g}{\partial \xi} + \rho_s v_s S + \frac{q_l}{\rho_l}c_l + (n-\theta)\left(v_{ai} + v_g\right)c_g, \tag{43}$$

where D_{ic} ($i = l, g$) is the hydrodynamic dispersion coefficient and the thermal diffusion effect is represented through the temperature-dependent diffusion coefficient in each phase. Here, the VOC advective flux in the gas phase has two parts: v_{ai} is driven by the air pressure gradient and the equivalent vapour diffusion velocity, and v_g is due to the water vapour density gradient. In previous studies, Thomas and Ferguson [10] took into account the first part, while Nassar and Horton [36] considered the second part. However, in general both of them should be incorporated, by analogy with the derivation of the water vapour transport equation.

When defining the total concentration of the VOCs (41) and their flux (43), the bulk density of the soil, ρ_{sb}, is often used to express the solute mass sorbed onto the solid phase [36, 8]. However, ρ_{sb} varies with porosity changes. Therefore, ρ_s is employed here, for convenience in explicitly describing the varying porosity.

The hydrodynamic dispersion coefficient for VOCs in the liquid phase, D_{lc}, is given by [36]:

$$D_{lc} = 0.001 D_0 \frac{e^{10\theta}}{\theta} + D_{hw}, \tag{44}$$

where $D_{hw} = \alpha_{Lw}|v_{li}|$ ($\alpha_{Lw} = 0.004$ m [53] is the longitudinal dispersivity) is the mechanical dispersion coefficient of the VOC. D_0 is the mass diffusivity of the organic chemical through water, and can be expressed through the Wilke–Chang equation [40] (which is also quoted by [36]):

$$D_0 = \frac{7 \times 10^{-12} \sqrt{\phi M_w}\,(T + T_0)}{\mu_w V_i^{0.6}}, \tag{45}$$

where ϕ is the dimensionless association factor of the solvent (2.6 for water [36]), M_w is the molecular weight of water, and V_i is the molal volume of organic solute at the normal boiling point, which can be estimated from additive methods [37] as 224 cm^3/mol and 98 cm^3/mol for toluene and benzene, respectively.

The dynamic viscosity of water, μ_w (mPa s), is [27]:

$$\mu_w = 661.2\,(T + T_0 - 229)^{-1.562}\,. \tag{46}$$

Liquid state theories for calculating diffusion coefficients are quite idealized and none can be considered as universally satisfactory for calculations [37]. Equation (45), which has an error around 10% [37] is one of the estimation methods for the binary liquid diffusion coefficient of a liquid at infinite dilution. .

The hydrodynamic dispersion coefficient for VOCs in the gas phase, D_{gc}, is [36]:

$$D_{gc} = \Omega D_{gm} + D_{hg}, \tag{47}$$

where $D_{hg} = \alpha_{Lg}|v_{ai}|$ (α_{Lg} is the dispersivity and is taken to be 1 cm [54] in this paper) is the dispersion coefficient of the VOC in the gas phase. The molecular-diffusion coefficient of an organic compound in a gaseous mixture (water vapour, air and VOC), D_{gm}, can be calculated via (25), while $\Omega = (n - \theta)^{2/3}$ is a factor representing the tortuosity. The binary diffusion diffusivity (m^2/s) for gas i through gas n in the vapour phase can be calculated from [55, 40, 37]:

$$D_{i-n} = \frac{1.43 \times 10^{-7} \left(T + T_0\right)^{1.75}}{P \left(M_{i-n}\right)^{1/2} \left[\left(\Sigma_v\right)_i^{1/3} + \left(\Sigma_v\right)_n^{1/3}\right]^2}, \tag{48}$$

where $M_{i-n} = 2\left(1/m_i + 1/m_n\right)^{-1}$, $m_j (j = i, n)$ (g/mol) is the molecular weight for the gases ($j = i, n$), Σ_v (no units) is the sum of the atomic diffusion volumes for each gas component [37] (18 for water vapour, 19.7 for dry air, 90.96 for benzene) and P is the air pressure ($= p_a$) with units in bar.

Since each VOC compound has a different specific gas constant (due to its unique molecular weight) and partitioning coefficient, one mass conservation equation can be written for each individual component when the VOCs are a multi-component mixture. There is no extra theoretical complexity except that more computational effort is required. In this paper, only a single compound is considered.

2.4. Moisture and heat energy transfer in the material coordinate system (z, t)

The mass balance equation for moisture is:

$$\begin{aligned}\frac{\partial}{\partial t}\left\{\left[\rho_l\theta + \rho_v\left(n-\theta\right)\right]M\right\} = -\frac{\partial}{\partial z}\Bigg[&-\rho_l k_l \frac{\partial}{\partial \xi}\left(p_c + p_a + \rho_l g \xi_i\right) - \rho_l D_T \frac{\partial T}{\partial \xi} \\ &-D^* \frac{\partial \rho_v}{\partial \xi} - \rho_v k_a \frac{\partial p_a}{\partial \xi}\Bigg],\end{aligned} \tag{49}$$

where M on the left hand side (LHS) accounts for deformation of a representative element volume (REV) relative to the spatial grid. The spatial gradient involved in the water flux on the right-hand side is implemented by transforming to the material coordinate system, i.e., $\partial(\cdot)/\partial\xi = M^{-1}\partial(\cdot)/\partial z$.

The mass balance equation for dry air is:

$$\frac{\partial}{\partial t}\left\{\rho_{da}\left[n-(1-H)\,\theta\right]M\right\}=-\frac{\partial}{\partial z}\left\{H\rho_{da}\left[-k_l\frac{\partial}{\partial\xi}\left(p_c+p_a+\rho_l g\xi_i\right)-D_T\frac{\partial T}{\partial\xi}\right]+\rho_{da}\left(-k_a\frac{\partial p_a}{\partial\xi}\right)\right\}. \tag{50}$$

397 Heat energy conservation gives:

$$\begin{aligned}\frac{\partial}{\partial t}(\Phi M)=-\frac{\partial}{\partial z}\Bigg\{&-\lambda\frac{\partial T}{\partial\xi}+\left[\left(-\rho_l k_l\frac{\partial}{\partial\xi}\left(p_c+p_a+\rho_l g\xi_i\right)-\rho_l D_T\frac{\partial T}{\partial\xi}\right)C_l\right.\\&+\left(-D^*\frac{\partial\rho_v}{\partial\xi}-\rho_v k_a\frac{\partial p_a}{\partial\xi}\right)C_v+\left(H\rho_{da}\left(-k_l\frac{\partial}{\partial\xi}(p_c+p_a+\rho_l g\xi_i)-D_T\frac{\partial T}{\partial\xi}\right)\right.\\&\left.\left.+\rho_{da}\left(-k_a\frac{\partial p_a}{\partial\xi}\right)\right)C_{da}\right]T+\left[-\rho_l k_l\frac{\partial}{\partial\xi}\left(p_c+p_a+\rho_l g\xi_i\right)-\rho_l D_T\frac{\partial T}{\partial\xi}\right]W\\&+L_0\left(-D^*\frac{\partial\rho_v}{\partial\xi}-\rho_v k_a\frac{\partial p_a}{\partial\xi}\right)-D_c^*\frac{\partial}{\partial\xi}\left(p_c+p_a+\rho_l g\xi_i\right)\Bigg\}.\end{aligned} \tag{51}$$

398 Mass conservation for the VOCs is given by:

$$\begin{aligned}\frac{\partial}{\partial t}\left(c_{mt}M\right)=-\frac{\partial}{\partial z}\Bigg\{&-\theta D_{lc}\frac{\partial c_l}{\partial\xi}-(n-\theta)\,D_{gc}\frac{\partial c_g}{\partial\xi}\\&-\left[k_l\frac{\partial}{\partial\xi}\left(p_c+p_a+\rho_l g\xi_i\right)+D_T\frac{\partial T}{\partial\xi}\right]c_l-k_a\frac{\partial p_a}{\partial\xi}c_g+\frac{D^*}{\rho_v}\frac{\partial\rho_v}{\partial\xi}c_g\Bigg\}.\end{aligned} \tag{52}$$

399 Equations (49–52) can also be developed via coordinate transformations. The
400 method for tackling v_s is analogous to that used in Appendix C of [13]. The proce-
401 dure is demonstrated in Appendix B. When $M = 1$, the equations can be reduced
402 to the geometric linear model without considering the soil velocity. Expanding
403 the terms on the LHS of each equation yields:

$$E_{11}\frac{\partial \sigma_v}{\partial t}+E_{12}\frac{\partial p_c}{\partial t}+E_{13}\frac{\partial p_a}{\partial t}+E_{14}\frac{\partial T}{\partial t}$$
$$=-\frac{\partial}{\partial z}\left[-\rho_l k_l\frac{\partial}{\partial \xi}\left(p_c+p_a+\rho_l g\xi_i\right)-\rho_l D_T\frac{\partial T}{\partial \xi}-D^*\frac{\partial \rho_v}{\partial \xi}-\rho_v k_a\frac{\partial p_a}{\partial \xi}\right], \tag{53}$$

$$E_{21}\frac{\partial \sigma_v}{\partial t}+E_{22}\frac{\partial p_c}{\partial t}+E_{23}\frac{\partial p_a}{\partial t}+E_{24}\frac{\partial T}{\partial t}$$
$$=-\frac{\partial}{\partial z}\left\{H\rho_{da}\left[-k_l\frac{\partial}{\partial \xi}\left(p_c+p_a+\rho_l g\xi_i\right)-D_T\frac{\partial T}{\partial \xi}\right]+\rho_{da}\left(-k_a\frac{\partial p_a}{\partial \xi}\right)\right\}, \tag{54}$$

$$\begin{aligned}
&E_{31}\frac{\partial \sigma_v}{\partial t}+E_{32}\frac{\partial p_c}{\partial t}+E_{33}\frac{\partial p_a}{\partial t}+E_{34}\frac{\partial T}{\partial t}\\
=&-\frac{\partial}{\partial z}\left\{-\lambda\frac{\partial T}{\partial \xi}+\left[-\rho_l k_l\frac{\partial}{\partial \xi}\left(p_c+p_a+\rho_l g\xi_i\right)-\rho_l D_T\frac{\partial T}{\partial \xi}\right]C_l T\right.\\
&+\left(-D^*\frac{\partial \rho_v}{\partial \xi}-\rho_v k_a\frac{\partial p_a}{\partial \xi}\right)C_v T+H\rho_{da}\left[-k_l\frac{\partial}{\partial \xi}\left(p_c+p_a+\rho_l g\xi_i\right)-D_T\frac{\partial T}{\partial \xi}\right]C_{da}T\\
&+\rho_{da}\left(-k_a\frac{\partial p_a}{\partial \xi}\right)C_{da}T+\left[-\rho_l k_l\frac{\partial}{\partial \xi}\left(p_c+p_a+\rho_l g\xi_i\right)-\rho_l D_T\frac{\partial T}{\partial \xi}\right]W\\
&\left.+L_0\left(-D^*\frac{\partial \rho_v}{\partial \xi}-\rho_v k_a\frac{\partial p_a}{\partial \xi}\right)-D_c^*\frac{\partial}{\partial \xi}\left(p_c+p_a+\rho_l g\xi_i\right)\right\},
\end{aligned} \tag{55}$$

and

$$E_{41}c_l\frac{\partial \sigma_v}{\partial t}+E_{42}c_l\frac{\partial p_c}{\partial t}+E_{43}c_l\frac{\partial p_a}{\partial t}+E_{44}c_l\frac{\partial T}{\partial t}+E_{45}\frac{\partial c_l}{\partial t}$$
$$\begin{aligned}
=&-\frac{\partial}{\partial z}\left\{\left[\theta D_{lc}+(n-\theta)D_{gc}H_{gl}\right]\frac{\partial c_l}{\partial \xi}-(n-\theta)D_{gc}\frac{\partial H_{gl}}{\partial \xi}c_l\right.\\
&\left.-\left[k_l\frac{\partial}{\partial \xi}\left(p_c+p_a+\rho_l g\xi_i\right)+D_T\frac{\partial T}{\partial \xi}\right]c_l-k_a\frac{\partial p_a}{\partial \xi}H_{gl}c_l-\frac{D^*}{\rho_v}\frac{\partial \rho_v}{\partial \xi}+H_{gl}c_l\right\}.
\end{aligned} \tag{56}$$

The coefficients E_{ij} ($i=1-4,\ j=1-5$) used in (53)–(56) are formulated in detail in Appendix A. The spatial coordinate ξ is determined by:

$$\xi = z + \int_z^L \frac{e_0 - e(\zeta)}{1 + e_0} d\zeta. \tag{57}$$

Thus, the first-order PDE:

$$\frac{\partial \xi}{\partial z} = 1 + \frac{e_0 - e(z)}{1 + e_0}, \tag{58}$$

with boundary conditions $\xi(L, t) = L$ was constructed to find ξ.

2.5. Constitutive relationships

A non-linear elastic soil model is used here. Generally, both state surfaces for the void ratio and the liquid water content can be postulated as [27]:

$$e = f_e(\sigma^*, p_c, T), \tag{59}$$

$$\theta = f_\theta(\sigma^*, p_c, T). \tag{60}$$

Considering (5), e and θ actually depend on the four primary variables. Thus, we have:

$$e = f_e(\sigma_v, p_c, p_a, T), \tag{61}$$

$$\theta = f_\theta(\sigma_v, p_c, p_a, T). \tag{62}$$

Lloret and Alonso [56] give an extensive review of a number of forms of state surfaces and concluded that the following formulation gives the best description of the soil behavior (also employed in [12]):

$$e = a + b\ln(-\sigma^*) + c\ln(-p_c) + d\ln(-\sigma^*)\ln(-p_c) + (1 + e_0)\alpha_T T, \quad (63)$$

where a, b, c, and d are model parameters. The thermal coefficient of volume change, α_T, can be expressed by [29]:

$$\alpha_T = \alpha_0 + \alpha_2 T + (\alpha_1 + \alpha_3 T)\ln\left(\frac{\sigma^*}{\sigma_0^*}\right). \quad (64)$$

Here, σ_0^* is the reference net mean stress and α_i $(i = 0, 1, 2, 3)$ are the model parameters.

The water retention curve and the hydraulic conductivity for a clay liner at a reference temperature of T_r can be described by [56] (employed in [30]):

$$\theta = \{a' - [1 - \exp(-b' p_c)](c' - d'\sigma^*)\}\frac{e}{1 + e}, \quad (65)$$

where a', b', c', and d' are model parameters.

The unsaturated hydraulic conductivity of a deformable soil under isothermal conditions, K_l, is given by [57]:

$$K_l = k_l \rho_l g = A\left(\frac{S_l - S_{lu}}{1 - S_{lu}}\right)^3 10^{\alpha_k e}, \quad (66)$$

where S_l is the degree of saturation and A, S_{lu}, and α_k are the related constants. The mobility coefficient of the continuous air phase, k_a, is [57]:

$$k_a = \frac{B}{\mu_a}[e(1 - S_l)]^\beta, \quad (67)$$

where μ_a is the dynamic viscosity of the pore air and B and β are model constants.

The governing equations are solved using the multiphysics modelling software package COMSOL 3.5a [58]. In the model, the spatial domains were discretized

into unstructured Lagrange-linear elements with a maximum global element size of 10^{-2} m, and maximum local element size at the end boundaries of 10^{-3} m. The sub-time steps were set to 1h and 1d in the two benchmark problems, respectively. The corresponding solutions have been confirmed to be independent on the sizes of time-steps and meshes.

To verify the present model, the model was reduced in order to be validated against benchmark problems in the literature. The first example is for the Isothermal moisture transport in a deformable soil column[27], while the second example is for the multi-phase VOC transport [8]. The compersions between the reduction from present model and the previous analytical solutions show an excellent agreement.

3. Application: VOC transport through an intact CCL

3.1. Problem description

The liner system investigated here is of a type widely used in waste impoundments and is assumed to be of sufficiently large extent to justify a one-dimensional analysis. As schematically shown in Figure 1, the composite landfill consists of an impermeable geomembrane impervious to the diffusion of an inorganic solute, an underlying clay soil layer such as an engineered compacted clay layer, and a second leachate collecting system. In this paper, only the CCL is modeled, the effects of the overlying geomembrane and the second leachate collecting system below CCL on the porous flow and VOCs transport are represented with proper boundary [13]. The CCL is assumed to be intact during the VOC breakthrough.

Initially, the VOC-free CCL has a uniform pore air pressure (1 bar) and temperature of T_0. To account for the initial steady liquid distribution with gravity, a linear variation of the pore water pressure is assumed as in [29]:

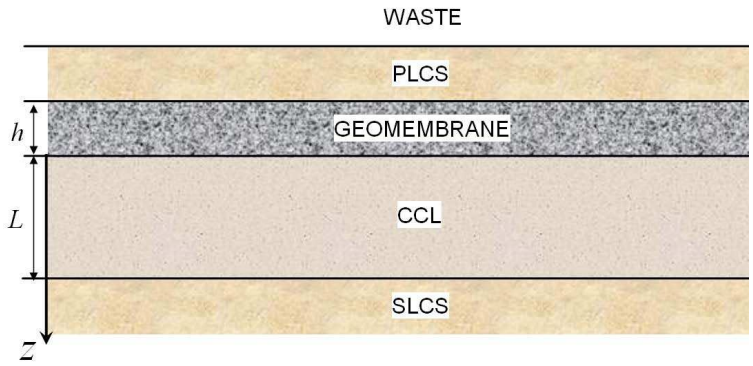

Figure 1: Schematic of a composite landfill liner [28].

$$p_c(z, t = 0) = p_{cr} + \rho_{l0} g_i (L - z) . \tag{68}$$

Here, p_{cr} is the reference capillary pressure and L is the thickness of the CCL. The initial uniform net mean stress is σ_0^*.

At the top of the CCL, a time-dependent temperature increase is imposed. It increases rapidly to a fixed value, and then decreases gradually to zero.

$$T(z = 0, t) = \begin{cases} t/t_1 \Delta T, & 0 \le t \le t_1 \\ \Delta T, & t_1 \le t \le t_2 \\ [1 - (t - t_2) / (t_3 - t_2)] \, \Delta T, & t_2 \le t \le t_3 \\ 0, & t \ge t_3 \end{cases} \tag{69}$$

Here, ΔT is the maximum temperature increase and t_i $(i = 1, 2, 3)$ are the times at which the temperature changes due to waste degradation.

The waste filling process is approximated by a linear ramp loading [13]:

$$\sigma_v(z=0,t) = \begin{cases} t/t'\Delta Q, & 0 \le t \le t' \\ \Delta Q. & t \ge t' \end{cases}, \tag{70}$$

where ΔQ is the maximum surcharge and t' is the time taken by the landfill to reach its full capacity.

The impervious geomembrane means that the liquid water mass flux equals zero, $q_l(z=0,t)=0$, and the pore air pressure gradient vanishes, i.e., $\partial p_a(z=0,t)/\partial z = 0$.

VOC vapour can permeate through a non-porous geomembrane at the molecular level. The process occurs in three steps [59, 60]. First, the permeant dissolves and partitions at the geomembrane surface. Second, it diffuses through the geomembrane in the direction of lower chemical potential. Finally, it evapourates or desorbs onto the ambient receiving medium.

The VOCs diffuse through the thin (relative to the CCL) geomembrane at the top boundary, with a flux given by:

$$f(0^-,t) = -P_G \frac{c_l(0^+,t) - c_0}{h}, \tag{71}$$

where c_0 is the concentration of the VOCs in the liquid phase at the top side of the geomembrane, which has a thickness of h_{GM}. P_G is the product of the diffusion coefficient for the solute in the geomembrane (D_G) and the partitioning coefficient of the solute between the geomembrane and the adjacent fluid (S_G) [14]. A good contact between the geomembrane and the CCL is assumed, and consequently $c_l(0^+,t)$ is the same as the concentration at the bottom surface of the geomembrane. Then, the flux in the CCL at the interface is:

$$f(0^+, t) = -\theta D_{lc} \frac{\partial c_l}{\partial z}(0^+, t). \tag{72}$$

Equating (71) and (72) [13], a Neumann boundary condition for the solute concentration is obtained:

$$\frac{\partial c_l}{\partial z}(0, t) - \frac{P_G}{\theta(0^+, t) h D_{lc}} c_f(0, t) = -\frac{P_G}{\theta(0^+, t) h D_{lc}} c_0. \tag{73}$$

At the bottom of the CCL, the second leachate collecting system is often made of gravel material with a high hydraulic conductivity. Therefore, the flow of pore water contained in the CCL driven by the capillary pressure and temperature gradients is assumed to drain freely and the gradient of the solute concentration is assumed to be zero (Danckwert's boundary condition, [61]), although different interpretations of this condition are possible (e.g., [62]):

$$\begin{aligned} &p_c(z = L, t) = p_c(z = L, t = 0), \\ &p_a(z = L, t) = 1 \text{ bar}, \\ &T(z = L, t) = T_0, \\ &\frac{\partial c_l}{\partial z} = 0. \end{aligned} \tag{74}$$

The model parameters employed in the following analyses are based on recent studies of solute transport in clay liners [63, 14]. The values of the parameters used are shown in Tables 1–4 unless stated otherwise.

The coupled non-linear equations are solved using the multiphysics modelling software package COMSOL 3.5a, which solves Equations (6), (53)–(56), and (58) simultaneously. Consequently, the two-way coupling of the moisture and the VOC

Table 1: Soil parameters employed in numerical simulations.

Parameter	Value
Initial concentration in the landfill, c_0	100 mg/dm^3
Maximum waste loading, ΔQ	2×10^5 Pa
Loading period, t'	2 y
Geomembrane thickness, h_{GM} [14]	0.0015 m
Mass transfer coefficient of geomembrane, P_G [14]	4×10^{-11}m^2/s
CCL thickness, L	1 m
Magnitude of acceleration due to gravity, g	9.81 m/s^2
Initial compressive stress, σ_{v0} [12]	-200 kPa
Reference capillary pressure, p_{cr} [12]	-2.8 kPa
Earth pressure coefficient at rest, K_0	0.9
Temperature coefficient of water retention, C_ψ [32]	-0.0068 K^{-1}
Temperature increase at the top boundary, ΔT	30 K
Initial temperature in the liner, T_0	288 K
Temperature changes parameters, t_i ($i = 1, 2, 3$)	1 y, 10 y and 10 y respectively

Table 2: Soil components properties.

Parameter	Value
Soil solids	
Density of the solid phase, ρ_s	2.7×10^3 kg/m^3
Specific heat capacity, $C_{p,s}$ [14]	800 J kg^{-1} K^{-1}
Soil liquid water	
Initial pore water density, ρ_{l0} [14]	0.998×10^3 kg/m^3
Phenomenological coefficient relating liquid flux to temperature, D_T [27]	2.7×10^{-10} m^2/(s K)
Reduction factor of surface tension due to VOC, γ_m/γ_w	0.8
Specific heat capacity, $C_{p,f}$ [14]	4180 J kg^{-1} K^{-1}
Soil air	
Henry's solubility coefficient for air, H [14]	0.02
VOC transport	
Specific gas constant for VOC, R_{VOC}	8.3144621/MW J/(kg K), where MW is molar weight of VOC (78.114 g/mol for Benzene)
Partitioning coefficient, H_{sg}	1.8×10^{-3} m^3/kg
Longitudinal mechanical dispersion coefficient for liquid phase, α_{Lw}	0.004 m

Table 3: State surface functions for unsaturated soil [12]

Void ratio	a	b	c	d	α_T (K^{-1})
	5.5	-0.4	-0.25	0.02	2.5×10^{-4}
Volumetric water content	a'	b'	c'	d'	
	0.9	-0.8	-10^{-8}	10^{-5}	

Table 4: Liquid mobility in unsaturated soil [12].

Hydraulic conductivity	A (m/s)	S_{lu}	α_k
	6×10^{-14}	0.05	5
Conductivity of air	B (Pa m/s)	μ_a (N s/m^2)	β_k
	1.8×10^{-12}	1.0×10^{-5}	4

transport is implemented. In the model, the system was discretized into unstructured Lagrange-linear elements with a maximum global element size of 10^{-2} m, and maximum local element size at the end boundaries (where the most rapid changes occur) of 10^{-3} m. The setting of sub-step size along the lines is corresponding to the waste filling process. The external loading increases from zero to its maximum in the first 2 y and then keeps steady. The sub-time step was set to 10^{-2} y in the simulation of the first 2 y, after which it was increased to 1 y in the following simulation period. All aforementioned time-steps and meshes have been checked through a convergence tests and then used in the following numerical examples.

3.2. Results and discussion

3.2.1. Geometric non-linearity and soil velocity

One of the important features of the present model (FD) is that it accounts for the finite deformation of the CCL, namely, the geometric non-linearity. In addition, the soil velocity is included. Two other models were constructed for comparison. The first one is a small deformation model (SD1), which does not incorporate the soil velocity occurrence in both the mass flux and the linear average velocity of the liquid phase v_{li} and v_{ai}. The second (SD2) is also a small deformation model, the difference with SD1 being that it considers the soil velocity.

As illustrated in Figure 2, the small deformation model underestimates the transit of the contaminant. Relative to the finite deformation model (FD), the small deformation models SD1 and SD2 assume that the thickness of the soil is constant even though consolidation causes soil contraction. As a result, it takes the VOCs longer to breakthrough the CCL. In previous research on non-isothermal moisture transport in deformable soil, the solid velocity was neglected based on the assumption that it is relatively small. However, Figure 2 demonstrates that including soil mobility can accelerate the transport of VOCs. It is noted that even with a small solid velocity, the capacity of the solid to transport solute ($(1-n)\rho_s v_s S$) may become non-negligible because of a relatively large solid density. Therefore, the present model not only is theoretically consistent by considering the soil velocity but also accommodates the geometric non-linearity.

Since there is a significant advective VOC flux (the advective flux is approximately 50 times the diffusive flux, especially when the temperature increases, ΔT is higher), the VOC concentration level at the exiting boundary may exceed that

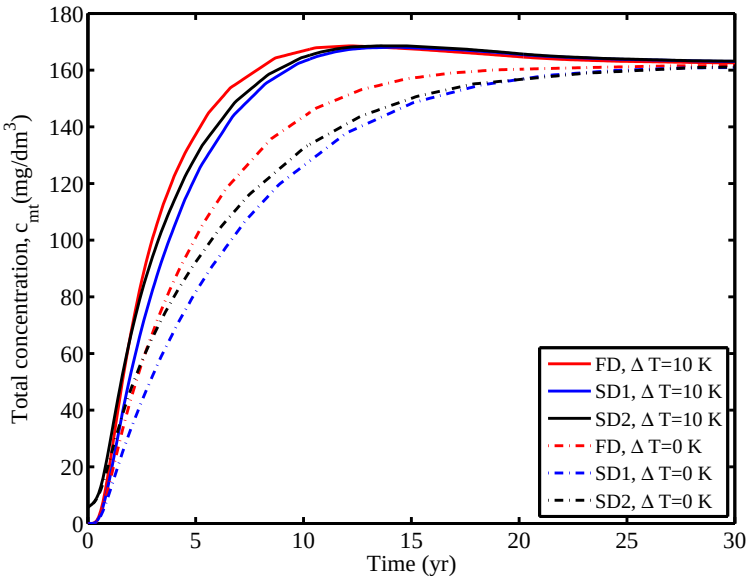

Figure 2: Effect of geometric non-linearity and soil velocity on VOCs breakthrough.

in its vicinity. With a temperature decrease, and an advective flux gradually vanishing, the VOC concentration at the bottom boundary gradually decreases due to the dispersion of mass to the adjacent zone, until steady state is reached.

3.2.2. Two-way coupling coefficient D^* and ρ_{da}

The water vapour diffusivity, D^*, can be calculated using (24), (25), (48), which we refer to as method WVD1. This approach requires two-way coupling of the moisture, heat, and the VOC transport to provide real-time values of the concentration of the VOCs when determining D^*. Alternatively, D^* can be approximated by (18) and (19) (method WVD2), so that the solution of the VOC transport can be decoupled and calculated sequentially after solving for the moisture and heat transport. However, Figure 3 demonstrates that WVD2 overestimates the water vapour diffusivity and predicts a faster contaminant migration as a result.

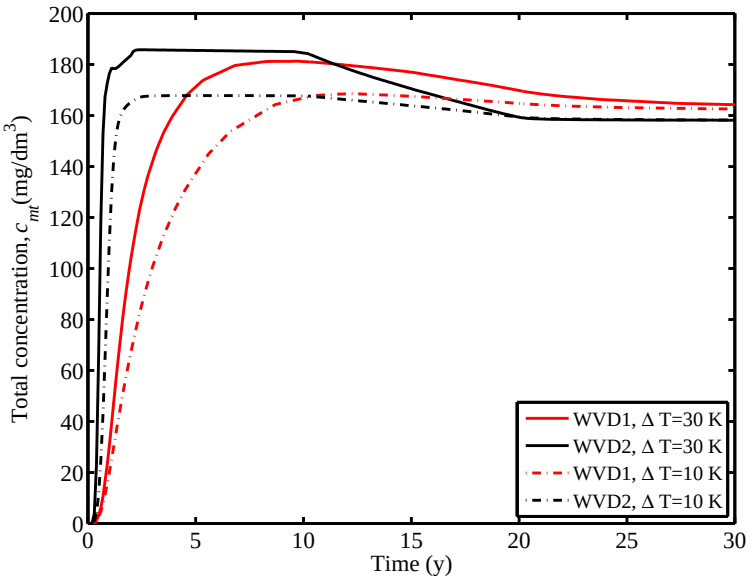

Figure 3: Effect of different methods for estimations of water vapour diffusivity on VOCs breakthrough.

For either WVD1 or WVD2, the final levels of the total VOC concentration are identical, regardless of the temperature gradient. As explained in the last section, the concentration level at the exit boundary undergoes a decrease, especially for a greater temperature gradient. This is probably caused by the relatively larger ratio of advection to the effective dispersion in the advection–dispersion equation. On the other hand, whether considering VOCs or not when calculating the density of dry air, ρ_{da} does not make a discernible difference on the VOC transport progress (results not shown).

3.2.3. Total constitution of the concentration of the VOCs

In the literature, there is no consensus on an expression for the total concentration of VOCs in unsaturated soil. While Thomas and Ferguson [10] only focused

on retention of VOCs in the aqueous and gaseous phases, most researchers consider that the VOCs also reside in the solid phase, due to sorption. However, different description are used. For example, some have described the sorbed concentration as being from either the aqueous or gaseous phases [64, 36], but others have included adsorption from both fluid phases [48, 8].

Figure 4 illustrates the liquid phase concentration and the total concentration level at the bottom boundary. 'ExpCtoti' represents three kinds of model: with the expression for the total concentration used in the present model ($i = 1$), excluding any contribution of adsorption from the gas phase ($i = 2$), and no adsorption onto the solid phase ($i = 3$). Although the liquid and gas phases are assumed to be in equilibrium in this study, it means that the transfer kinetic comes to a steady state, namely the concentration of the VOCs in one phase can be evaluated from that in another phase. However, the concentration in liquid and gas phases are not necessary to be identical. Therefore, the sorption was separated from both the liquid and gas phases

As expected, the more complete adsorption mechanism results in slower VOC transport due to retardation. The difference of the final total concentrations in Figure 4(b) caused by their different constitutions are significant. Therefore, more experiments are needed to clarify which expression of the adsorption is appropriate. A higher temperature increase at the top boundary leads to a larger carrying capacity of both the liquid and gas phases. Consequently, the migration of the VOCs is accelerated.

3.2.4. Longitudinal mechanical dispersion (D_{hw} and D_{hg})

Based on the assumption that the pore water flow velocity in fine-grained soils due to mechanical consolidation is low (less than 10^{-6} m/s), mechanical dispersion can be neglected [65, 14]. However, Zhang et al. [28] confirmed that the

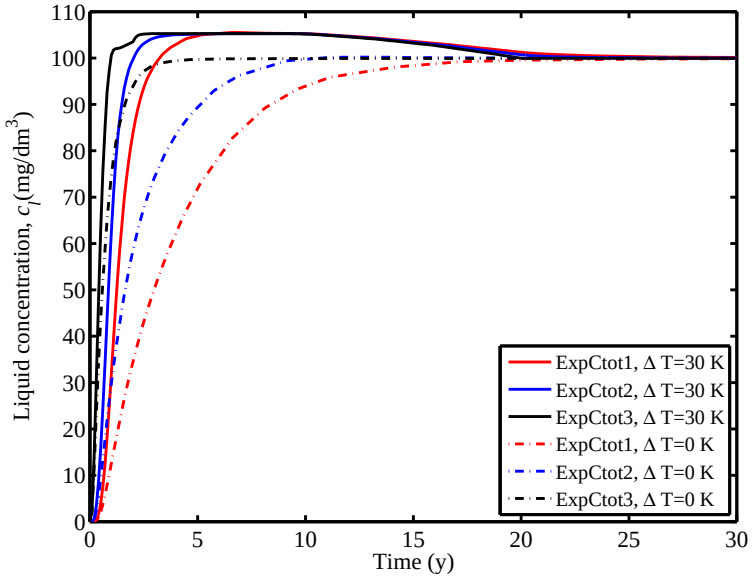

(a)

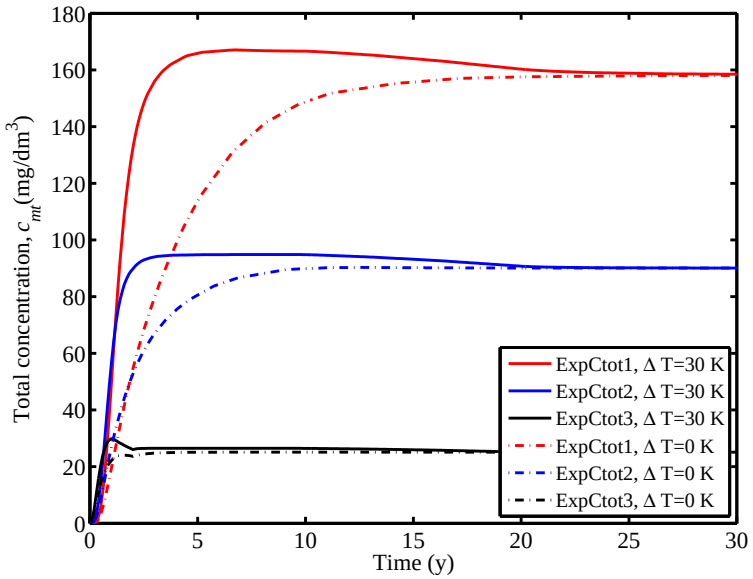

(b)

Figure 4: Comparison of the different expressions for the total VOC concentration on the predicted breakthrough.

mechanical dispersion could double the final advective emission at the bottom of a partially saturated CCL when the molecular diffusion coefficient decreases within a practical range. In this section, the effect of mechanical dispersion on VOC transport is reexamined in a multi-phase context.

The mechanical dispersivity is often obtained by fitting measured breakthrough curves with analytical solutions of the advection–dispersion equation. However, there is the so-called dispersion-scale effect, namely, the dispersivity changes with the distance over which the contaminants travel. A good first approximation is to use a value of one-tenth of the transport distance for the longitudinal dispersivity if there is not enough information [66]. In this section, α_{Lw} = 0.1 m[67] was used to examine the effect of mechanical dispersion.

Figure 5 illustrates the distribution of the VOCs' dispersive flux in both the aqueous and gaseous phases. For the unsaturated soil considered here, the gas molecular diffusive flux is over four orders greater than the gas mechanical dispersivity flux, so the mechanical dispersive flux is small compared with the dominant diffusive flux through the gas phase (which is at the scale of 10^{-6} g/(m^2 s)). Therefore, the mechanical dispersion in unsaturated CCL in the considered cases can be neglected (as shown in Figure 6).

3.2.5. Mechanical consolidation and temperature increase

When the waste is added at the top boundary, the clay liner undergoes mechanical consolidation, which can cause advective pore flow and thus is expected to help accelerate VOC transit. To investigate the contribution of mechanical consolidation in an unsaturated CCL, the present model was reduced to 'NoSV', which does not include variation of the vertical stress. A comparison was made between it and the present model (Model Cpt). Figure 7a and the case with ΔT= 30 K in

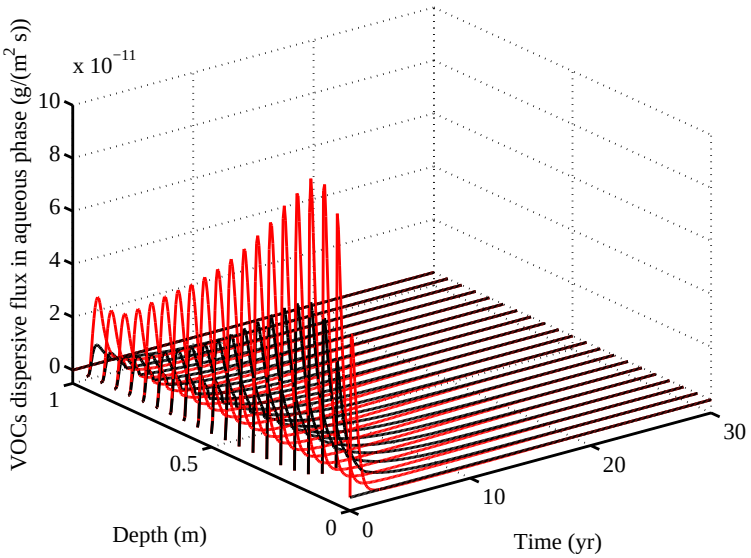

(a) Aqueous phase flux

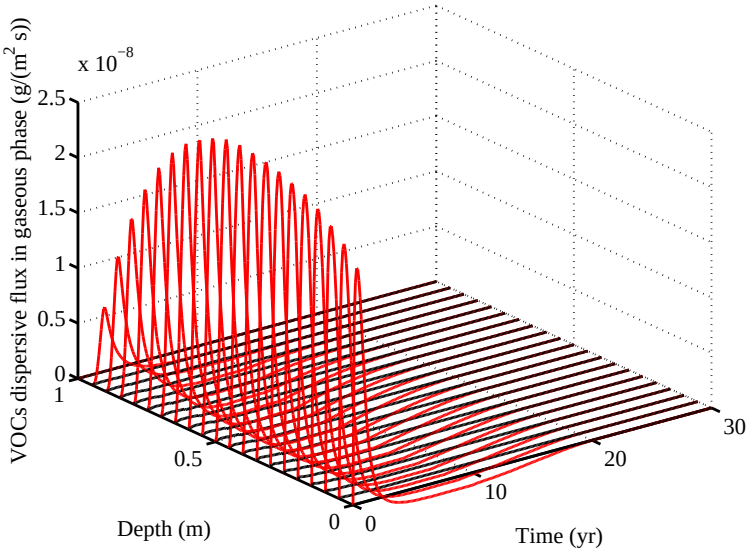

(b) Gaseous phase flux

Figure 5: Distribution of VOCs' dispersive flux (α_{Lw} = 0.1 m): red curves for T = 30 K and black curves for T = 0 K.

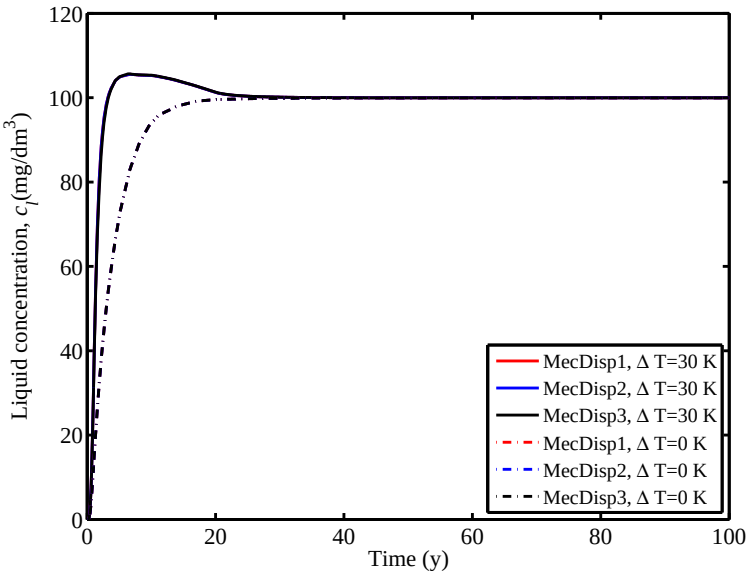

Figure 6: Effect of mechanical dispersion on VOC breakthrough (α_{Lw} = 0.1 m).

Figure 7b demonstrate that including the vertical compressive stress, namely, the mechanical consolidation, seems to predict a slower transport of the VOCs, which is contrary to the conclusion for their transport (in the solid and liquid phases) within a saturated or partially saturated CCL. This is due to two effects: First, the gas phase diffusion dominates the transport progress for unsaturated soil instead of the advective flux in the liquid phase for saturated soil; second, the mechanical consolidation compacts the CCL and reduces the effective gas diffusion due to the lower void ratio. For the cases with larger temperature gradients, the effect of soil contraction due to mechanical consolidation is balanced by the swelling due to heating. Thus, the influence of mechanical consolidation on the movement of the VOCs is limited. Furthermore, both the liquid phase concentration and the total concentration of the VOCs at higher temperature gradients have higher peak values than at lower temperature gradients. This phenomenon is a result of the

advective transport due the higher temperature gradient. Gradually, the concentration level decreases with decreasing advective fluxes of the VOCs.

In Figure 7b, the total concentration for 'Model Cpt' surpasses that of 'Model NoSV' for cases with ΔT= 0 K after a certain period. This is because the total sorptive capacity of a unit volume of solid is greater than that of a unit volume of pore fluid. When the soil is compressed and the void fluid is expelled, a unit volume of soil can carry more VOCs. Therefore, mechanical consolidation does not always lead to a faster transit of multi-phase VOCs within an unsaturated soil.

Figure 8 indicates that the lower pre-consolidation stress and the consequent larger initial void can speed the migration of the VOCs. Three pre-consolidation stress levels are considered here: PS1 with $\sigma_{v0} = -200$ kPa, PS2 with $\sigma_{v0} = -100$ kPa, and PS3 with $\sigma_{v0} = -50$ kPa. The values of the corresponding initial void ratio are 0.628 (0.646), 0.775 (0.815) and 0.920 (0.980), respectively. The values in brackets are the void ratios at the CCL bottom (the void ratio increases linearly from top to bottom due to the distribution of the initial capillary pressure).

A higher temperature increase at the top boundary was observed to shorten significantly the time required for breakthrough. This is because the gas phase VOC diffusion increases rapidly with increasing temperature and dominates the migration progress.

3.2.6. Contribution of the gaseous phase

In this section, a model (NoGas) without VOC flux in the gas phase is setup by letting $H_{gl} = H_{sg} = 0$ in the present model. As illustrated in Figure 9, incorporating the gas phase can dramatically speed up the migration of VOCs for both non-isothermal and isothermal soils. This is attributed to the greater magnitude of

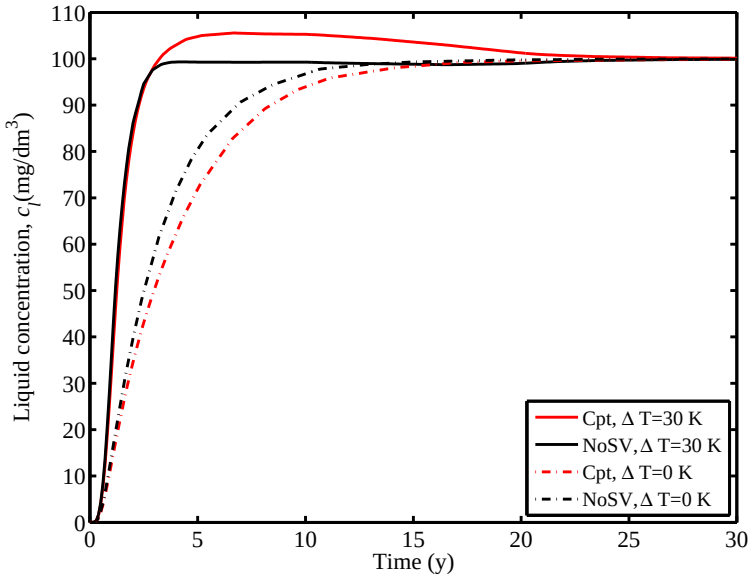

(a)

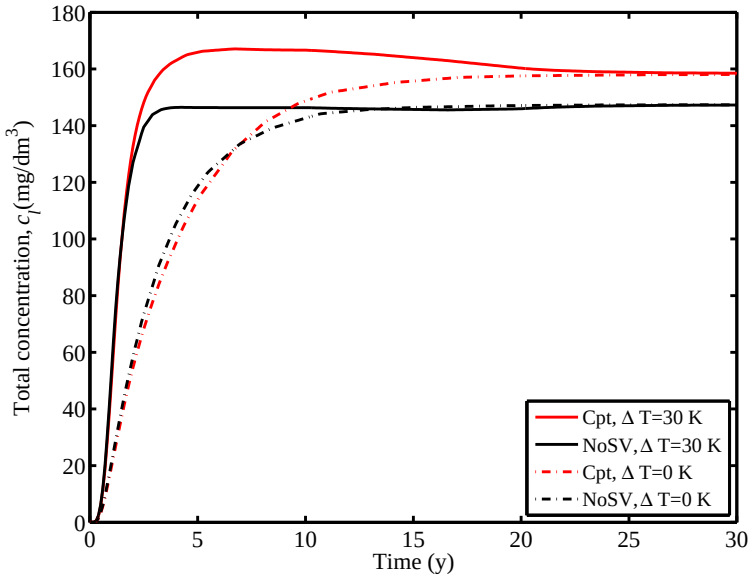

(b)

Figure 7: Effect of mechanical consolidation and temperature increase on VOC breakthrough.

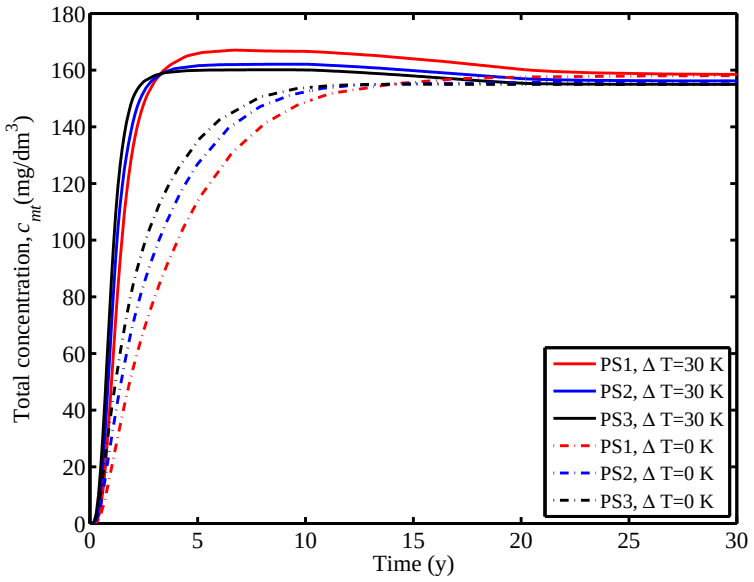

Figure 8: Effect of pre-consolidation stress (σ_{v0}) and temperature increase on VOC breakthrough ($a' = 0.9$).

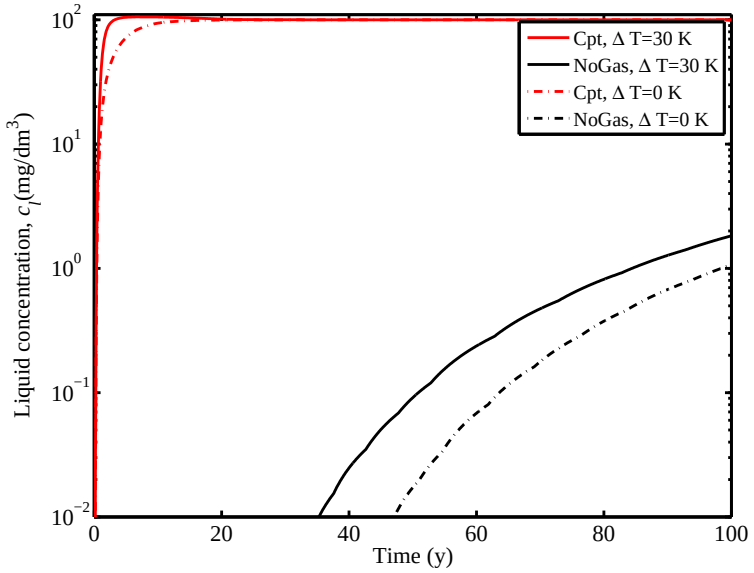

Figure 9: Contribution of the gas phase to VOC breakthrough ($a' = 0.9$).

the diffusion coefficient (around 10^{-7} m^2/s) for the gas phase relative to that for the fluid phase (around 10^{-10} m^2/s).

Since gas phase diffusion depends on the gas saturation, $S_g = 1 - \theta/n$, a parametric study on the initial volume water content, θ, was performed to examine the influence of the degree of saturation on VOC migration. Figure 10 shows that lower water content leads to faster VOC migration in unsaturated soil, predicted by three-phase transport model, which is in the opposite direction to the trend for the two-phase (aqueous and solid phases) model (NoGas). In the former model, a lower water content means a larger gas saturation and a larger gas flow pathway. In contrast, it results in a smaller pore water fraction, which impedes the VOC transit according to the model NoGas.

Therefore, gas phase transport plays a crucial role in the VOC transport within unsaturated soil. As reported in the literature, some researchers attributed the observed faster VOCs breakthrough than the estimation of the pure-diffusion model to the mechanical consolidation of soil liner [13, 68]. However, other researchers [14, 15] suggested that the influence of mechanical consolidation on solute transport was not important, especially when the compressibility is low and decreasing of hydrodynamic dispersion due to soil compression is significant. The present results redirect our attention to examine whether the soil liner is fully saturated. If it is not, the gaseous phase VOCs transport could be a primary reason for accelerated VOC transport.

4. Conclusions

A one-dimensional non-isothermal multi-phase (solid, liquid, and gas phases) moisture and VOC transport model for a non-linear elastic porous medium was

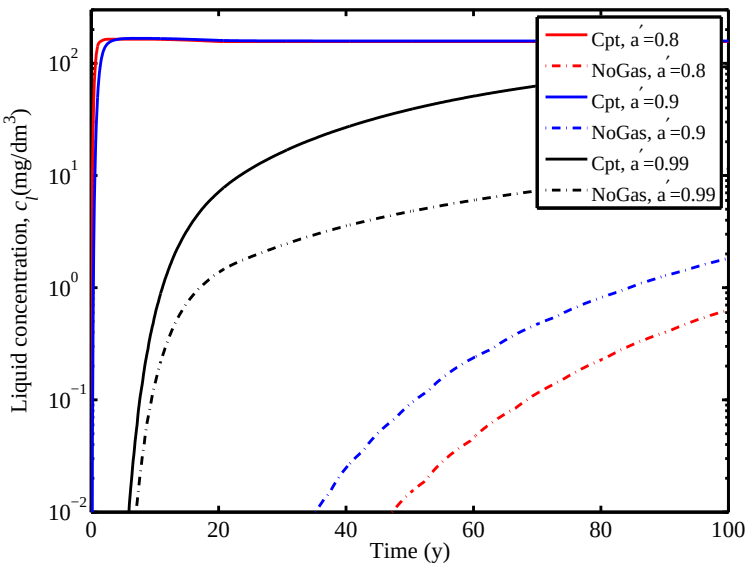

Figure 10: Effect of water content on VOC breakthrough: Solid line is the present model and dash-dot line is for the NoGas model.

developed. The model proposed in this study is theoretically consistent for a deformable soil column by including the soil velocity in the linear average pore fluid (liquid and gas) velocities and taking into account the mass flux due to the motion of the soil. Based on the present model, benzene migration in a solid waste landfill CCL under top surcharge and temperature gradient conditions was investigated. Mainly, the following conclusions can be drawn:

1. The assumption of small deformations (neglecting changes of the soil column) and ignoring the motion of the soil underestimates the transit of the VOCs;
2. A two-way coupling approach is essential to get an accurate determination of the water vapour diffusion coefficient in the presence of VOC vapour;

3. Taking into account the adsorption of the VOCs from both the gas and fluid phases in the composition of the total concentration can considerably slow down the migration progress predicted by the model;
4. The mechanical dispersion of the fluid phase can be neglected because the related VOC dispersion fluxes are several orders of magnitude less than the diffusive flux in the gas phase.
5. The shrinking of the pores in the soil due to mechanical consolidation helps to prevent VOC breakthrough, but a higher environmental temperature increases the VOC gas phase diffusion, which plays a predominant role in an unsaturated soil liner.
6. Furthermore, the deviation of saturation from the fully saturated state can significantly speed up the motion of VOCs. Therefore, a non-isothermal multi-phase moisture and VOC transport model is essential to obtain a reliable prediction of the migration of VOCs in an unsaturated soil liner exposed to heating and compression.

References

[1] J. Y. Kim, Migration of volatile organic compounds from the landfill liner systems, Environmental Engineering Research 2 (1997) 233–243.

[2] T.-B. Nguyen, J. Lim, H. Choi, T. D. Stark, Numerical modeling of diffusion for volatile organic compounds through composite landfill liner systems, KSCE Journal of Civil Engineering 15 (2011) 1033–1039.

[3] S. G. Fityus, D. W. Smith, J. R. Booker, Contaminant transport through an unsaturated soil liner beneath a landfill, Canadian Geotechnical Journal 36 (1999) 330–354.

[4] W. A. Jury, D. Russo, G. Streile, H. El-Abd, Evaluation of volatilization by organic chemicals residing below the soil surface, Water Resources Research 26 (1990) 13–20.

[5] I. Nassar, L. Ukrainczyk, R. Horton, Transport and fate of volatile organic chemicals in unsaturated, nonisothermal, salty porous media: 2. experimental and numerical studies for benzene, Journal of Hazardous Materials 69 (1999) 169 – 185.

[6] R. K. Rowe, Long-term performance of contaminant barrier systems, Geotechnique 55 (2005) 631–678.

[7] J. Philip, D. De Vries, Moisture movement in porous materials under temperature gradients, Transactions of the American Geophysical Union 38 (1957) 222–232.

[8] C. Shan, D. B. Stephens, An analytical solution for vertical transport of volatile chemicals in the vadose zone, Journal of Contaminant Hydrology 18 (1995) 259 – 277.

[9] I. N. Nassar, R. Horton, Heat, water, and solution transfer in unsaturated porous media: I. theory development and transport coefficient evaluation, Transport in Porous Media 27 (1997) 17–38.

[10] H. R. Thomas, W. J. Ferguson, A fully coupled heat and mass transfer model incorporating contaminant gas transfer in an unsaturated porous medium, Computers and Geotechnics 24 (1999) 65–87.

[11] H. R. Thomas, Y. He, A coupled heat-moisture transfer theory for deformable unsaturated soil and its algorithmic implementation, International Journal for Numerical Methods in Engineering 40 (1997) 3421–3441.

[12] Y. Zhou, R. K. Rowe, Modeling of clay liner desiccation, International Journal of Geomechanics, ASCE 5 (2005) 1–9.

[13] G. P. Peters, D. W. Smith, Solute transport through a deforming porous medium, International Journal for Numerical and Analytical Methods in Geomechanics 26 (2002) 683–717.

[14] T. W. Lewis, P. Pivonka, D. W. Smith, Theoretical investigation of the effects of consolidation on contaminant transport through clay barriers, International Journal For Numerical And Analytical Methods In Geomechanics 33 (2009) 95–116.

[15] H. Zhang, D.-S. Jeng, D. Barry, B. Seymour, L. Li, Solute transport in nearly saturated porous media under landfill clay liners: A finite deformation approach, Journal of Hydrology 479 (2013) 189–199.

[16] J. E. Bogner, J. P. Chanton, D. Blake, Effectiveness of a florida landfill biocover for reduction of ch4 and nmhc emissions, Environmental Science and Technology 44 (2010) 1197–1203.

[17] C. Scheutz, J. Bogner, J. Chanton, D. Blake, M. Morcet, Atmospheric emissions and attenuation of non-methane organic compounds in cover soils at a french landfill, Waste Management 28 (2008) 1892–1908.

[18] C. Schuetz, J. Bogner, J. Chanton, Comparative oxidation and net emissions of methane and selected mon-methane organic compounds in landfillcover soils, Environmental Science and Technology 37 (2003) 5150–5158.

[19] B. E. Sleep, Modeling transient organic vapor transport in porous media with the dusty gas model, Advances in Water Resources 22 (1998) 247–256.

[20] C.-S. Fen, W. Liang, P. Hsiesh, Y. Huang, Knudsen and molecular diffusion coefficients for gas transport in unconsolidated porous media, Soil Science Society of America Journal 75 (2011) 456–467.

[21] A. Geiges, Examination of the assumption of thermal equilibrium on the fluid distribution and front stability, Ph.D. thesis, Institut fur Wasserbau, Universitat Stuttgart, Germany (2009).

[22] J. L. Boyd, V. Sivakumar, Experimental observations of the stress regime in unsaturated compacted clay when laterally confined, Géotechnique 61 (4) (2011) 345–363.

[23] D. Fredlund, H. Rahardjo, Soil Mechanics for Unsaturated Soils, Wiley, 1993.

[24] K. Ishihara, At-rest and compaction-induced lateral earth pressures of moist soils, Ph.D. thesis, Civil engineering, Virginia Polytechnic Institute and State University, Blacksburg, Virginia, USA (1993).

[25] T. B. Edil, A review of aqueous-phase voc transport in modern landfill liners, Waste Management 23 (2003) 561–571.

[26] J. Bear, A. H.-D. Cheng, Modeling Groundwater Flow and Contaminant Transport, Springer, Heidelberg, 2010.

[27] Y. Zhou, R. K. N. D. Rajapakse, Coupled heat-moisture-are transport in deformable unsaturated media, Journal of Engineering Mechanics 24 (1998) 1090–1099.

[28] H. J. Zhang, D.-S. Jeng, B. R. Seymour, D. A. Barry, L. Li, Solute transport in partially-saturated deformable porous media: Application to a landfill clay liner, Advances in Water Resources 40 (2012) 1–10.

[29] H. Thomas, Y. He, M. Sansom, C. Li, On the development of a model of the thermo-mechanical-hydraulic behaviour of unsaturated soils, Engineering Geology 41 (1996) 197– 218.

[30] F. M. Azad, A. El-Zein, R. K. Rowe, D. W. Airey, Modelling of thermally induced desiccation of geosynthetic clay liners in double composite liner system, Geotextiles and Geomembranes 34 (2012) 28–38.

[31] P. Milly, A simulation analysis of thermal effects on evaporation from soil, Water Resources Research 20 (1984) 1087–1098.

[32] B. Scanlon, P. Milly, Water and heat fluxes in desert soils, 2. numerical simulations, Water Resources Research 30 (1994) 721–733.

[33] Y. Zhou, R. K. Rowe, Development of a technique for modelling clay liner desiccation, International Journal for Numerical and Analytical Methods in Geomechanics 27 (2003) 473–493.

[34] H. R. Thomas, S. D. King, A non-linear, two-dimensional, potential based analysis of coupled heat and mass transfer in a porous medium, Int. J. Numer. Meth. Engng 37 (1994) 3707–3722.

[35] J. E. Smith, R. W. Gillham, The effect of concentration-dependent surface tension on the flow of water and transport of dissolved organic compounds: a pressure head-based formulation and numerical model, Water Resources Research 30 (1994) 343–354.

[36] I. Nassar, R. Horton, Transport and fate of volatile organic chemicals in unsaturated, nonisothermal, salty porous media: 1. theoretical development, Journal of Hazardous Materials 69 (1999) 151 – 167.

[37] R. Reid, J. Prausintz, B. Poling, The Properties of Gases and Liquids, McGraw-Hill, New York, 1987.

[38] R. Tuckermann, Surface tension of aqueous solutions of water-soluble organic and inorganic compounds, Atmospheric Environment 41 (2007) 6265–6275.

[39] R. Tuckermann, H. K. Cammenga, The surface tension of aqueous solutions of some atmospheric water-soluble organic compounds, Atmospheric Environment 38 (2004) 6135–6138.

[40] J. Welty, C. Wicks, R. E. Wilson, Foundamentals of Momentum, Heat, and Mass Transfer, 3 rd Ed., John Wiley & Sons, New Jersey, USA, 1984.

[41] H. R. Thomas, M. R. Sansom, Fully coupled analysis of heat, moisture and air transfer in unsaturated soil, Journal of Engineering Mechanics, ASCE 121 (1995) 392–405.

[42] J. Challa, D. Skoff, F. J. Quirus, Landfill gas as source of vocs in ground water, Practice Periodical of Hazardous, Toxic, and Radioactive Waste Management 1 (2) (1997) 61–75.

[43] A. Hodgson, K. Garbesi, R. Sextro, J. Daisey, Soil-gas contamination and entry of volatile organic compounds into a house near a landfill, Air and Waste Management 42 (1992) 277–283.

[44] H. Soltani-Ahmadi, A review of the literature regarding non-methane and volatile organic compounds in municipal solid waste landfill gas, Tech. rep., Department of Civil Enviromental Engineering, University of Delaware, Newark, USA (2000).

[45] L. Prunty, Spatial distribution of heat of wetting in porous media, in: 2002 ASAE Annual International Meeting / CIGR XVth World Congress, Sponsored by ASAE and CIGR, Chicago, Illinois, USA, 2002.

[46] B. D. Kay, P. H. Groenevelt, On the interaction of water and heat in frozen and unfrozen solids: I. basic theory-the vapor phase, Soil Science Society of America 38 (1974) 395–400.

[47] P. C. D. Milly, Moisture and heat transport in hysteretic, inhomogeneous porous media: A matric heat-based formulation and a numerical model, Water Resources Research 18 (1982) 489–498.

[48] T. G. Poulsen, P. Moldrup, T. Yamaguchi, J. W. Massmann, J. A. Hansen, Voc vapor sorption in soil: soil type dependent model and implications for vapor extraction, Journal of Environmental Engineering 124 (1998) 146–155.

[49] L. W. Petersen, P. Moldrup, Y. EI-Farhan, O. H. Jacobsen, T. Yamaguchi, D. E. Rolston, The effect of moisture and soil texture on the adsorption of organic vapors, Journal of Enviromental Quality 24 (1995) 752–759.

[50] C. K. Ho, Gas Transport in Porous Media, Springer, 2006, Ch. 4, pp. 47–54.

[51] J. Staudinger, P. V. Roberts, A critical compilation of henry's law constant temperature dependence relations for organic compounds in dilute aqueous solutions, Chemosphere 44 (2001) 561–576.

[52] T. G. Poulsen, J. W. Massmann, P. Moldrup, Effects of vapor extraction on contaminant flux to atmosphere and ground water, Journal of Enviromental Engineering 122 (1996) 700–706.

[53] R. Yong, A. Mohamed, B. Warkentin, Principles of contaminant transport in soils, Elsevier Science, New York, USA, 1992.

[54] D. Cann, W. Stiver, R. Zytner, Correlating gas phase dispersion and moisture content in undisturbed and disturbed unsaturated soils, in: RemTech 2004 Proceedings, Environmental Services Association of Alberta (ESAA), 2004.

[55] E. Fuller, P. Schettler, J. Giddings, A new method for prediction of binary gas-phase diffusion coefficients, Industrial and Engineering Chemistry 58 (1966) 18–27.

[56] A. Lloret, E. E. Alonso, State surfaces for partially saturated soils, in: Proc. 11th I.C.S.M.F.E., Vol. 2, San Francisco, 1985, pp. 557–562.

[57] E. E. Alonso, F. Battle, A. Gens, A. Lloret, Consolidation analysis of partially saturated soils-application to earth dam construction, in: Proc., 6th International Conference of Numerical Methods Geomechanics, Innsbruck, 1988, pp. 1303–1308.

[58] COMSOL, COMSOL Multiphysics, 3rd Edition (May 2013).

[59] P. Pierson, M. Barroso, A ”pouch test” for characterizing gas permeability of geomembranes, Geosynthetics International 9 (2002) 345–372.

[60] T. D. Stark, H. Choi, Methane gas migration through geomembranes, Geosynthetics International 12 (2005) 120–126.

[61] P. V. Danckwerts, Continuous flow systems : Distribution of residence times, Chemical Engineering Science 2 (1953) 1–13.

[62] D. A. Barry, G. Sposito, Application of the convection-dispersion model to solute transport in finite soil columns, Soil Science Society of America Journal 52 (1988) 3–9.

[63] G. J. Foose, Transit-time design for diffusion through composite liners, Journal of Geotechnical and Geoenvironmental Engineering 128 (2002) 590–601.

[64] J.-S. Lin, L. M. Hildemann, A nonsteady-state analytical model to predict gaseous emissions of volatile organic compounds from landfills, Journal of Hazardous Materials 40 (1995) 271–295.

[65] Y. B. Acar, L. Haider, Transport of low-concentration contaminants in saturated earthen barriers, Journal of Geotechnical Engineering, ASCE 116 (1990) 1031–1052.

[66] M. Anderson, Movement of contaminants in groundwater: Groundwater transport-advection and dispersion, in: Groundwater Contamination, Studies in Geophysics, National Academy Press, Washington, DC., 1984, pp. 37–45.

[67] D. F. Yule, W. R. Gardner, Longitudinal and transverse dispersion coefficients in unsaturated plainfield sand, Water Resources Research 14 (1978) 582–588.

[68] G. P. Peters, D. W. Smith, The influence of advective transport on coupled chemical and mechanical consolidation of clays, Mechanics of Materials 36 (2004) 467–486.

Appendix A: The coefficients used in the governing equations

The coefficients E_{ij} ($i = 1-4,\ j = 1-5$) used in (53)–(56) are given as follows. For the case of a finite deformation, i.e., $M \neq 1$,

$$E_{11} = \frac{1+2K_0}{3}\left[\frac{1+e}{1+e_0}\left(\rho_l-\rho_v\right)\frac{\partial\theta}{\partial\sigma^*}+\frac{1}{1+e_0}\left(\rho_l\theta+\rho_v-\rho_v\theta\right)\frac{\partial e}{\partial\sigma^*}\right], \tag{75}$$

$$\begin{aligned} E_{12} = {} & \theta\frac{1+e}{1+e_0}\frac{\partial\rho_l}{\partial p_c}+\left(\frac{e}{1+e_0}-\theta\frac{1+e}{1+e_0}\right)\frac{\partial\rho_v}{\partial p_c} \\ & +\frac{1+e}{1+e_0}\left(\rho_l-\rho_v\right)\frac{\partial\theta}{\partial p_c}+\frac{1}{1+e_0}\left(\rho_l\theta+\rho_v-\rho_v\theta\right)\frac{\partial e}{\partial p_c}, \end{aligned} \tag{76}$$

$$E_{13} = \theta\frac{1+e}{1+e_0}\frac{\partial\rho_l}{\partial p_a} + \left(\frac{e}{1+e_0} - \theta\frac{1+e}{1+e_0}\right)\frac{\partial\rho_v}{\partial p_a} + E_{11}\frac{3}{1+2K_0}, \tag{77}$$

$$\begin{aligned} E_{14} = {} & \theta\frac{1+e}{1+e_0}\frac{\partial\rho_l}{\partial T} + \left(\frac{e}{1+e_0} - \theta\frac{1+e}{1+e_0}\right)\frac{\partial\rho_v}{\partial T} \\ & + \frac{1+e}{1+e_0}(\rho_l - \rho_v)\frac{\partial\theta}{\partial T} + \frac{1}{1+e_0}(\rho_l\theta + \rho_v - \rho_v\theta)\frac{\partial e}{\partial T}, \end{aligned} \tag{78}$$

$$E_{21} = \frac{1+2K_0}{3}\left(-(1-H)\rho_{da}\frac{1+e}{1+e_0}\frac{\partial\theta}{\partial\sigma^*} + \frac{\rho_{da}}{1+e_0}[1-(1-H)\theta]\frac{\partial e}{\partial\sigma^*}\right), \tag{79}$$

$$\begin{aligned} E_{22} = {} & \left[\frac{e}{1+e_0} - (1-H)\theta\frac{1+e}{1+e_0}\right]\frac{\partial\rho_{da}}{\partial p_c} - (1-H)\rho_{da}\frac{1+e}{1+e_0}\frac{\partial\theta}{\partial p_c} \\ & + \frac{\rho_{da}}{1+e_0}[1-(1-H)\theta]\frac{\partial e}{\partial p_c}, \end{aligned} \tag{80}$$

$$E_{23} = \left[\frac{e}{1+e_0} - (1-H)\theta\frac{1+e}{1+e_0}\right]\frac{\partial\rho_{da}}{\partial p_a} + E_{21}\frac{3}{1+2K_0}, \tag{81}$$

$$\begin{aligned} E_{24} = {} & \left[\frac{e}{1+e_0} - (1-H)\theta\frac{1+e}{1+e_0}\right]\frac{\partial\rho_{da}}{\partial T} - (1-H)\rho_{da}\frac{1+e}{1+e_0}\frac{\partial\theta}{\partial T} \\ & + \frac{\rho_{da}}{1+e_0}[1-(1-H)\theta]\frac{\partial e}{\partial T}, \end{aligned} \tag{82}$$

$$E_{31} = \frac{1+2K_0}{3}\left(E_{311}\frac{\partial e}{\partial\sigma^*} + E_{312}\frac{\partial\theta}{\partial\sigma^*}\right), \tag{83}$$

$$\begin{aligned} E_{311} = {} & L_0\frac{\rho_v}{1+e_0} - L_0\frac{\rho_v\theta}{1+e_0} + W\rho_l\frac{\theta}{1+e_0} + C_lT\rho_l\frac{\theta}{1+e_0} \\ & + C_vT\frac{\rho_v}{1+e_0} - C_vT\frac{\rho_v\theta}{1+e_0} + C_{da}T\frac{\rho_{da}}{1+e_0}[1-(1-H)\theta], \end{aligned} \tag{84}$$

$$E_{312} = -L_0\frac{\rho_v(1+e)}{1+e_0} + W\rho_l\frac{1+e}{1+e_0} + C_lT\rho_l\frac{1+e}{1+e_0} - C_vT\frac{\rho_v(1+e)}{1+e_0} - C_{da}T(1-H)\rho_{da}\frac{1+e}{1+e_0} + \rho_l\theta\frac{1+e}{1+e_0}\frac{\partial W}{\partial\theta}, \tag{85}$$

$$E_{32} = E_{321}\frac{\partial\rho_v}{\partial p_c} + E_{322}\frac{\partial\rho_l}{\partial p_c} + C_{da}T\left[\frac{e}{1+e_0} - (1-H)\theta\frac{1+e}{1+e_0}\right]\frac{\partial\rho_{da}}{\partial p_c} + E_{311}\frac{\partial e}{\partial p_c} + E_{312}\frac{\partial\theta}{\partial p_c}, \tag{86}$$

$$E_{321} = L_0\frac{e}{1+e_0} - L_0\frac{(1+e)\theta}{1+e_0} + C_vT\frac{e}{1+e_0} - C_vT\frac{(1+e)\theta}{1+e_0}, \tag{87}$$

$$E_{322} = W\frac{(1+e)\theta}{1+e_0} + C_lT\frac{(1+e)\theta}{1+e_0} + \rho_l\theta\frac{1+e}{1+e_0}\frac{\partial W}{\partial\rho_l}, \tag{88}$$

$$E_{33} = E_{321}\frac{\partial\rho_v}{\partial p_a} + E_{322}\frac{\partial\rho_l}{\partial p_a} + C_{da}T\left[\frac{e}{1+e_0} - (1-H)\theta\frac{1+e}{1+e_0}\right]\frac{\partial\rho_{da}}{\partial p_a} + E_{31}\frac{3}{1+2K_0}, \tag{89}$$

$$E_{34} = E_{321}\frac{\partial\rho_v}{\partial T} + E_{322}\frac{\partial\rho_l}{\partial T} + C_{da}T\left[\frac{e}{1+e_0} - (1-H)\theta\frac{1+e}{1+e_0}\right]\frac{\partial\rho_{da}}{\partial T} + E_{311}\frac{\partial e}{\partial T} + E_{312}\frac{\partial\theta}{\partial T} + C_s\frac{\rho_s}{1+e_0} + \left[C_l\rho_l\theta\frac{1+e}{1+e_0} + C_v\rho_v\left(\frac{e}{1+e_0} - \theta\frac{1+e}{1+e_0}\right)\right] + C_{da}\frac{\rho_{da}}{1+e_0}[e-(1-H)\theta(1+e)] \tag{90}$$

and

$$E_{41} = \frac{1+2K_0}{3}\left[E_{411}\frac{\partial e}{\partial\sigma^*} + E_{412}\frac{\partial\theta}{\partial\sigma^*} + \frac{\rho_s}{1+e_0}c_l\frac{\partial H_{sl}}{\partial\sigma^*} + \frac{1}{1+e_0}\rho_s c_l\frac{\partial\left(H_{sg}H_{gl}\right)}{\partial\sigma^*} + \frac{\partial\xi}{\partial z}(n-\theta)\,c_l\frac{\partial H_{gl}}{\partial\sigma^*},\right], \tag{91}$$

where

$$E_{411} = \frac{\theta}{1+e_0} c_l + H_{gl} c_l \frac{1-\theta}{1+e_0}, \tag{92}$$

$$E_{412} = \frac{\partial \xi}{\partial z} c_l - H_{gl} c_l \frac{\partial \xi}{\partial z}, \tag{93}$$

$$\begin{aligned} E_{42} =& E_{411} \frac{\partial e}{\partial p_c} + E_{412} \frac{\partial \theta}{\partial p_c} + \frac{\rho_s}{1+e_0} c_l \frac{\partial H_{sl}}{\partial p_c} \\ &+ \frac{\rho_s}{1+e_0} c_l \frac{\partial \left(H_{sg} H_{gl} \right)}{\partial p_c} + \frac{\partial \xi}{\partial z} (n-\theta) c_l \frac{\partial H_{gl}}{\partial p_c}, \end{aligned} \tag{94}$$

$$E_{43} = \frac{3}{1+2K_0} E_{41}, \tag{95}$$

$$\begin{aligned} E_{44} =& E_{411} \frac{\partial e}{\partial T} + E_{412} \frac{\partial \theta}{\partial T} + \frac{\rho_s}{1+e_0} c_l \frac{\partial H_{sl}}{\partial T} \\ &+ \frac{\rho_s}{1+e_0} c_l \frac{\partial \left(H_{sg} H_{gl} \right)}{\partial T} + \frac{\partial \xi}{\partial z} (n-\theta) c_l \frac{\partial H_{gl}}{\partial T} \end{aligned} \tag{96}$$

and

$$E_{45} = \frac{\rho_s}{1+e_0} \left(H_{sl} + H_{sg} H_{gl} \right) + \theta \frac{\partial \xi}{\partial z} + (n-\theta) \frac{\partial \xi}{\partial z} H_{gl}. \tag{97}$$

For small strain deformations, i.e., $M = 1$,

$$E'_{11} = \frac{1+2K_0}{3} \left[(\rho_l - \rho_v) \frac{\partial \theta}{\partial \sigma^*} + \rho_v (1+e)^{-2} \frac{\partial e}{\partial \sigma^*} \right], \tag{98}$$

$$E'_{12} = \theta \frac{\partial \rho_l}{\partial p_c} + (n-\theta) \frac{\partial \rho_v}{\partial p_c} + (\rho_l - \rho_v) \frac{\partial \theta}{\partial p_c} + \rho_v (1+e)^{-2} \frac{\partial e}{\partial p_c}, \tag{99}$$

$$E'_{13} = \theta\frac{\partial \rho_l}{\partial p_a} + (n-\theta)\frac{\partial \rho_v}{\partial p_a} + E'_{11}\frac{3}{1+2K_0}, \tag{100}$$

$$E'_{14} = \theta\frac{\partial \rho_l}{\partial T} + (n-\theta)\frac{\partial \rho_v}{\partial T} + (\rho_l - \rho_v)\frac{\partial \theta}{\partial T} + \rho_v (1+e)^{-2}\frac{\partial e}{\partial T}, \tag{101}$$

$$E'_{21} = \frac{1+2K_0}{3}\left[-(1-H)\rho_{da}\frac{\partial \theta}{\partial \sigma^*} + \rho_{da}(1+e)^{-2}\frac{\partial e}{\partial \sigma^*}\right], \tag{102}$$

$$E'_{22} = [n-(1-H)\theta]\frac{\partial \rho_{da}}{\partial p_c} - (1-H)\rho_{da}\frac{\partial \theta}{\partial p_c} + \rho_{da}(1+e)^{-2}\frac{\partial e}{\partial p_c}, \tag{103}$$

$$E'_{23} = [n-(1-H)\theta]\frac{\partial \rho_{da}}{\partial p_a} + E'_{21}\frac{3}{1+2K_0}, \tag{104}$$

$$E'_{24} = [n-(1-H)\theta]\frac{\partial \rho_{da}}{\partial T} - (1-H)\rho_{da}\frac{\partial \theta}{\partial T} + \rho_{da}(1+e)^{-2}\frac{\partial e}{\partial T}, \tag{105}$$

$$E'_{31} = \frac{1+2K_0}{3}\left(E'_{311}\frac{\partial e}{\partial \sigma^*} + E'_{312}\frac{\partial \theta}{\partial \sigma^*}\right), \tag{106}$$

$$E'_{311} = T(1+e)^{-2}(\rho_v C_v + \rho_{da}C_{da}) + L_0\rho_v(1+e)^{-2}, \tag{107}$$

$$E'_{312} = T[\rho_l C_l - \rho_v C_v - \rho_{da}C_{da}(1-H)] - L_0\rho_v + W\rho_l + \rho_l\theta\frac{\partial W}{\partial \theta} \tag{108}$$

and

$$E'_{32} = E'_{321}\frac{\partial \rho_v}{\partial p_c} + E'_{322}\frac{\partial \rho_l}{\partial p_c} + C_{da}T\left[n-(1-H)\,\theta\right]\frac{\partial \rho_{da}}{\partial p_c} + E'_{311}\frac{\partial e}{\partial p_c} + E'_{312}\frac{\partial \theta}{\partial p_c}, \tag{109}$$

where

$$E'_{321} = (n-\theta)\,(L_0 + C_v T)\,, \tag{110}$$

$$E'_{322} = (W + TC_l)\,\theta + \rho_l \theta \frac{\partial W}{\partial \rho_l}, \tag{111}$$

$$E'_{33} = E'_{321}\frac{\partial \rho_v}{\partial p_a} + E'_{322}\frac{\partial \rho_l}{\partial p_a} + C_{da}T\left[n-(1-H)\,\theta\right]\frac{\partial \rho_{da}}{\partial p_a} + E'_{31}\frac{3}{1+2K_0}, \tag{112}$$

$$E'_{34} = E'_{321}\frac{\partial \rho_v}{\partial T} + E'_{322}\frac{\partial \rho_l}{\partial T} + C_{da}T\left[n-(1-H)\,\theta\right]\frac{\partial \rho_{da}}{\partial T} + E'_{311}\frac{\partial e}{\partial T} + E'_{312}\frac{\partial \theta}{\partial T} + C_s\rho_s\,(1-n) + C_l\rho_l\theta + C_v\rho_v\,(n-\theta) + C_{da}\rho_{da}\left[n-(1-H)\,\theta\right] \tag{113}$$

and

$$E'_{41} = \frac{1+2K_0}{3}\left[E'_{411}\frac{\partial e}{\partial \sigma^*} + E'_{412}\frac{\partial \theta}{\partial \sigma^*} + E'_{413}\frac{\partial H_{sl}}{\partial \sigma^*} + E'_{413}\frac{\partial\left(H_{sg}H_{gl}\right)}{\partial \sigma^*} + E'_{414}\frac{\partial H_{gl}}{\partial \sigma^*}\right], \tag{114}$$

where

$$E'_{411} = c_l\,(1+e)^{-2}\left[\rho_s\left(H_{sl} + H_{sg}H_{gl}\right) + H_{gl}\right] \tag{115}$$

$$E'_{412} = c_l\left(1 - H_{gl}\right), \tag{116}$$

$$E'_{413} = c_l\left(1 - n\right)\rho_s, \tag{117}$$

$$E'_{414} = c_l\left(n - \theta\right), \tag{118}$$

$$E'_{42} = E'_{411}\frac{\partial e}{\partial p_c} + E'_{412}\frac{\partial \theta}{\partial p_c} + E'_{413}\frac{\partial H_{sl}}{\partial p_c} + E'_{413}\frac{\partial\left(H_{sg}H_{gl}\right)}{\partial p_c} + E'_{414}\frac{\partial H_{gl}}{\partial p_c}, \tag{119}$$

$$E'_{43} = \frac{3}{1 + 2K_0}E'_{41}, \tag{120}$$

$$E'_{44} = E'_{411}\frac{\partial e}{\partial T} + E'_{412}\frac{\partial \theta}{\partial T} + E'_{413}\frac{\partial H_{sl}}{\partial T} + E'_{413}\frac{\partial\left(H_{sg}H_{gl}\right)}{\partial T} + E'_{414}\frac{\partial H_{gl}}{\partial T} \tag{121}$$

and

$$E'_{45} = \left(1 - n\right)\rho_s\left(H_{sl} + H_{sg}H_{gl}\right) + \theta + \left(n - \theta\right)H_{gl}. \tag{122}$$

Appendix B: Coordinate conversion for the governing equations

As an example, consider the transformation of the moisture mass balance equation (15) from (ξ, t) coordinates to (z, t) coordinates. Inserting (8–11) into (15) yields

$$\begin{aligned}\frac{\partial}{\partial t}\left[\rho_l\theta + \rho_v\left(n - \theta\right)\right] = -\frac{\partial}{\partial \xi}\Bigg[&-\rho_l k_l\frac{\partial}{\partial \xi}\left(p_c + p_a + \rho_l g\xi_i\right) - \rho_l D_T\frac{\partial T}{\partial \xi} + \rho_l\theta v_s \\ &-D^*\frac{\partial \rho_v}{\partial \xi} - \rho_v k_a\frac{\partial p_a}{\partial \xi} + \rho_v\left(n - \theta\right)v_s\Bigg].\end{aligned} \tag{123}$$

Apply the transformation formula (1) and multiply both sides by M to get

$$\frac{\partial \xi}{\partial z}\frac{\partial}{\partial t}\left[\rho_l\theta+\rho_v(n-\theta)\right]-v_s\frac{\partial}{\partial \xi}\left[\rho_l\theta+\rho_v(n-\theta)\right]\frac{\partial \xi}{\partial z}$$
$$=-\frac{\partial}{\partial z}\left[-\rho_l k_l\frac{\partial}{\partial \xi}(p_c+p_a+\rho_l g\xi_i)-\rho_l D_T\frac{\partial T}{\partial \xi}\right. \tag{124}$$
$$\left.-D^*\frac{\partial \rho_v}{\partial \xi}-\rho_v k_a\frac{\partial p_a}{\partial \xi}\right]-\left[\rho_l\theta+\rho_v(n-\theta)\right]\frac{\partial v_s}{\partial z}-v_s\frac{\partial}{\partial z}\left[\rho_l\theta+\rho_v(n-\theta)\right].$$

The first term on the LHS and the second term on the right-hand side can be simplified using the product rule of differentiation,

$$\frac{\partial}{\partial t}\left[\rho_l\theta+\rho_v(n-\theta)\frac{\partial \xi}{\partial z}\right]=-\frac{\partial}{\partial z}\left[-\rho_l k_l\frac{\partial}{\partial \xi}(p_c+p_a+\rho_l g\xi_i)-\rho_l D_T\frac{\partial T}{\partial \xi}\right.$$
$$\left.-D^*\frac{\partial \rho_v}{\partial \xi}-\rho_v k_a\frac{\partial p_a}{\partial \xi}\right], \tag{125}$$

which is with the same as (49).

Nomenclature

a_0, a constant used in calculating the density of the vapour at saturation

A, a constant used in calculating the hydraulic conductivity

b_0, a constant used in calculating the density of the vapour at saturation

B, a constant used in calculating the mobility coefficient for the pore air

b, soil body force, $ML^{-2}T^{-2}$

C_l, specific heat capacity of pore liquid in soil, $L^2T^{-2}K^{-1}$

C_{da}, specific heat capacity of dry air in soil, $L^2T^{-2}K^{-1}$

C_v, specific heat capacity of water vapour in soil, $L^2T^{-2}K^{-1}$

C_ψ, the temperature coefficient of water retention, K^{-1}

c_{mt}, mass of contaminants per unit volume of soil matrix, ML^{-3}

c_l, VOC concentration in the liquid phase

c_g, VOC concentration in the gas phase

D_{atm}, the molecular diffusion coefficient of water vapour in air, L^2T^{-1}

D_0, mass diffusivity of organic chemical in water, L^2T^{-1}

D^*, effective molecular diffusivity of water vapour, L^2T^{-1}

D_{hg}, mechanical dispersion coefficient of the gas phase, L^2T^{-1}

D_{hw}, mechanical dispersion coefficient of the VOC, L^2T^{-1}

D_{lc}, hydrodynamic dispersion coefficient for the VOCs in the liquid phase, L^2T^{-1}

D_{gc}, hydrodynamic dispersion coefficient for the VOCs in the gas phase, L^2T^{-1}

D_{i-n}, molecular diffusivity for the binary pair, L^2T^{-1}

D_T, phenomenological coefficient relating the water flux to the temperature gradient, $L^2T^{-1o}K^{-1}$

D_{wm}, molecular diffusivity of water vapour in a gas mixture, L^2T^{-1}

e, void ratio

e_0, initial void ratio

P_G, mass transfer coefficient of the geomembrane, L^2T^{-1}

g, magnitude of acceleration due to gravity, LT^{-2}

g_i, gravity acceleration vector, LT^{-2}

h, relative humidity

h_{GM}, thickness of the geomembrane, L

K_l, hydraulic conductivity, LT^{-1}

k_a, mobility coefficient for gas, L^2TM^{-1}

k_l, mobility coefficient for liquid, L^2TM^{-1}

H, dimensionless solubility coefficient

$H_{ij}(i, j = s, l, g)$, linear partitioning coefficients between the individual soil phases

H_w, a constant in calculating the heat of wetting, MT^{-2}

K_0, earth pressure coefficient at rest

L_0, latent heat of vapourization, L^2T^{-2}

L, thickness of the CCL, L

M, Jacobian of a coordinate transformation

M_{i-n}, equivalent molecular weight, $Mmol^{-1}$

$m_j(j = i, n)$, molecular weight for the gas component, $Mmol^{-1}$

n, current soil porosity

n_0, initial soil porosity

P, air pressure with units in atmospheres

p_a, gauge pore air pressure, $ML^{-1}T^{-2}$

p_c, capillary pressure, $ML^{-1}T^{-2}$

p_{cr}, reference capillary pressure in the CCL, $ML^{-1}T^{-2}$

ΔQ, maximum surcharge, $ML^{-1}T^{-2}$

q_{ct}, total VOC flux, $ML^{-2}T^{-1}$

q_l, liquid water flux, $ML^{-2}T^{-1}$

q_T, heat flux, MT^{-3}

q_v, water vapour flux, $ML^{-2}T^{-1}$

R_{da}, specific gas constant for dry air, $L^2T^{-2}K^{-1}$

R_v, specific gas constant for water vapour, $L^2T^{-2}K^{-1}$

R_{VOC}, specific gas constant for VOC vapour, $L^2T^{-2}K^{-1}$

S, VOC concentration adsorbed to solid phase

S', specific surface of the material, L^{-1}

S_l, degree of saturation

t, time, T

T, temperature increase, K

ΔT, maximum temperature increase, K

T_r, an arbitrary reference temperature, K

T_0, initial temperature, K

v_{ai}, average air velocity, LT^{-1}

v_g, equivalent vapour diffusion velocity, LT^{-1}

v_{li}, average fluid velocity, LT^{-1}

v_s, solid velocity, LT^{-1}

W, differential heat of wetting, L^2T^{-2}

y'_n, the mole fraction of component n in the gas mixture

z, material coordinate, L

Greek symbols

ξ, spatial coordinate, L

λ, equivalent thermal conductivity of unsaturated soil, $MLT^{-3}K^{-1}$

λ_{dry}, thermal conductivity of completely dry soil, $MLT^{-3}K^{-1}$

λ_{sat}, thermal conductivity of fully saturated soil, $MLT^{-3}K^{-1}$

Γ_0, superficial volume fraction of water in the surface layer

Γ_w, superficial volume fraction of VOC in the surface layer

γ_0, surface tension of the VOC, $ML^{-3}T^{-2}$

γ_w, surface tension of a free-water system at the reference temperature, $ML^{-3}T^{-2}$

γ_m, surface tension of pore water in the presence of VOCs, $ML^{-3}T^{-2}$

σ^*, net mean soil stress, $ML^{-1}T^{-2}$

σ_0^*, initial uniform net mean stress in the CCL, $ML^{-1}T^{-2}$

σ_l, lateral soil stress, $ML^{-1}T^{-2}$

σ_v, vertical soil stress, $ML^{-1}T^{-2}$

ρ_{da}, density of dry air, ML^{-3}

ρ_0, density of vapour at saturation, ML^{-3}

ρ_l, density of the pore liquid, ML^{-3}

ρ_{l0}, initial density of the pore liquid, ML^{-3}

ρ_s, density of the soil grains, ML^{-3}

ρ_v, density of water vapour, ML^{-3}

ρ_{VOC}, density of VOC vapour, ML^{-3}

α_k, a constant to calculate the hydraulic conductivity

α_l, thermal expansion coefficient for pore water, K^{-1}

α_{Lg}, longitudinal dispersivity parameter for the gas phase, L

α_{Lw}, longitudinal dispersivity parameter for the liquid phase, L

β, a constant used in calculating the mobility coefficient for pore air

β_l, pore water compressibility coefficient, Pa^{-1}

δ, a constant in calculating the heat of wetting, L

ν_m, the mass flow factor

τ, dimensionless tortuosity factor

θ, volume water content

θ_0, initial volume water content

Ψ, capillary potential head, L

$\Psi(T_r)$, the capillary pressure head at the reference temperature, L

Φ, heat capacity of the soil, $ML^{-1}T^{-2}$

ϕ, dimensionless association factor of a solvent

μ_a, dynamic viscosity of the pore air, MT^{-1}

μ_w, dynamic viscosity of the pore water, MT^{-1}

Ω, factor representing the tortuosity in calculating the dispersion coefficient of the VOCs in the gas phase

Σ_v, sum of the atomic diffusion volumes for each gas component